

Presentation for my PhD thesis in France and my postdoc in Czech Republic

Chun-Lu Huang

ISS, Academia Sinica

Group meeting, ISS,
AS, Taipei, 27/08/2021



My Ph.D. program in France

- Studied in IJClab at Université de Paris-Saclay, France
- Period from Oct. 2017 to Oct. 2020
- Supported by Ministry of Education, M.O.E, Taiwan and Université de Paris-Saclay (教育部世界百大合設獎學金)
- Publication:
 - C.-L. Huang, Inclusive J/ ψ production in pp and Pb-Pb collisions at $\sqrt{s_{\text{NN}}} = 5.02 \text{ TeV}$ with ALICE at the LHC, [CERN-THESIS-2021-001](#)
 - C.-L. Huang, Recent results on heavy flavor in small and large systems from ALICE, [PoS \(LHCP2020\) 036](#), [arXiv: 2010.12469 \[hep-ex\]](#)
 - C.-L. Huang, Inclusive J/ ψ production in pp and Pb-Pb collisions at $\sqrt{s_{\text{NN}}} = 5.02 \text{ TeV}$ with ALICE at the LHC, JRJC 2019 Book of Proceedings



université
PARIS-SACLAY



My postdoc fellowship in Czech Republic

- Worked in the electron acceleration group at ELI Beamlines, Czech Republic
- Period from Nov. 2020 to May. 2021
- Supported by the institute of Physics of the Czech Academy of Sciences
- Duty:
 - Develop a data acquisition system for the laser experiment
 - Develop machine learning algorithms for post-processing of the experimental data
 - Implement the online analysis within the ELI-Beamlines control system and laser teams

Content

- LHC and ALICE
- Data analysis in pp and Pb-Pb collisions at $\sqrt{s_{\text{NN}}} = 5.02 \text{ TeV}$
 - Analysis steps
 - Results
- ELI-Beamlines
- Development of data acquisition system

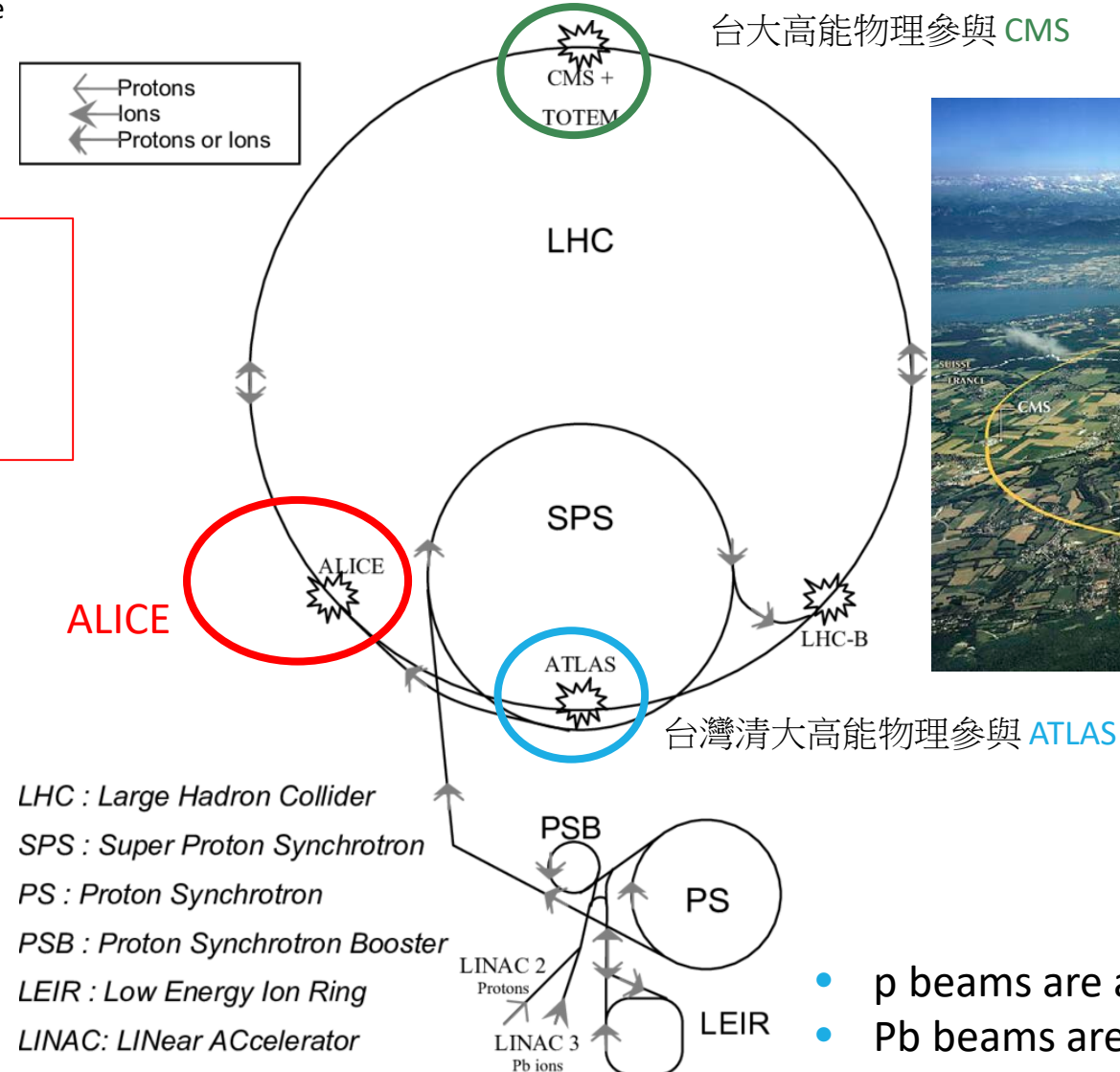
LHC and ALICE

Large Hadron Collider and A Large Ion Collider Experiment

CERN* accelerator complex and beam

*: Conseil Européen pour la Recherche Nucléaire

- ALICE was designed to study Quark Gluon Plasma (QGP) in Pb-Pb. Physics in pp and p-Pb collisions are also studied.



CERN-THESIS-2006-012
(Figure is not at scale)

台大高能物理參與 CMS

Figure from [wiki](#)



- p beams are accelerated up to 6.5 TeV.
- Pb beams are accelerated up to 2.51 A TeV

Confined and deconfined nuclear matter

A proton consists of u quarks of 2 and a d quark. A neutron has a u quark and d quarks of 2.

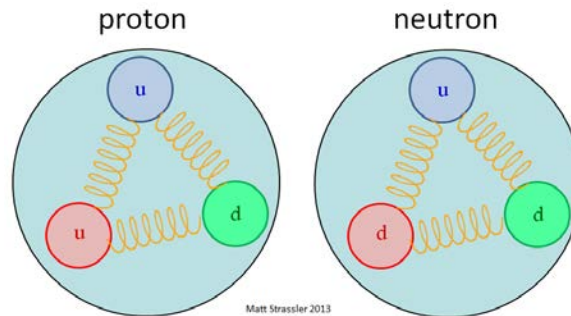


Figure from [online resource](#)

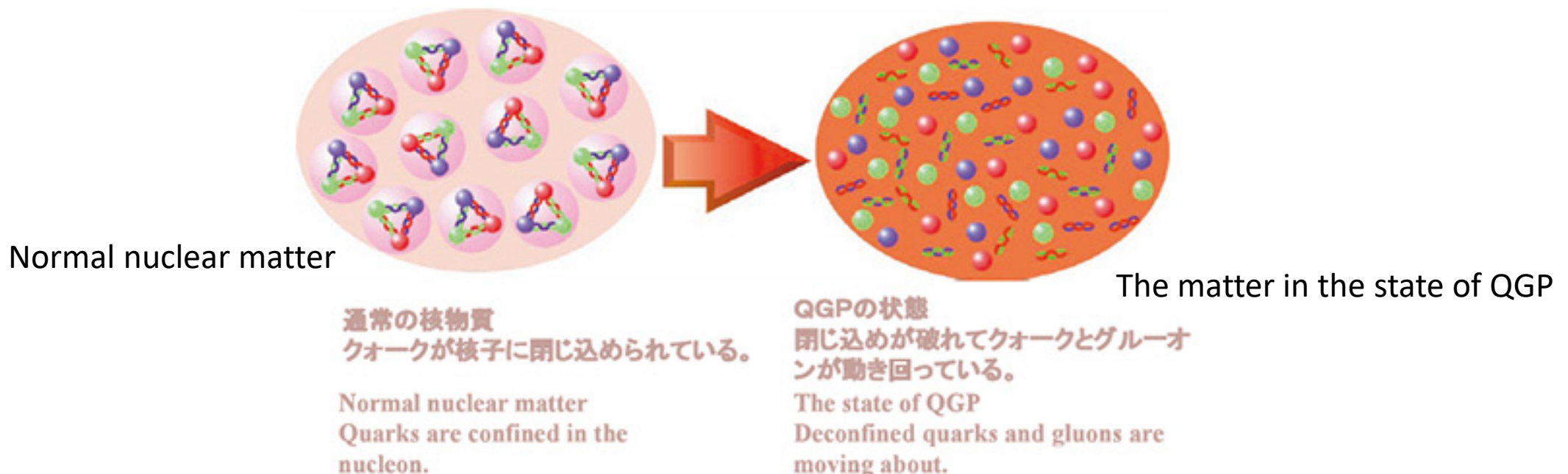
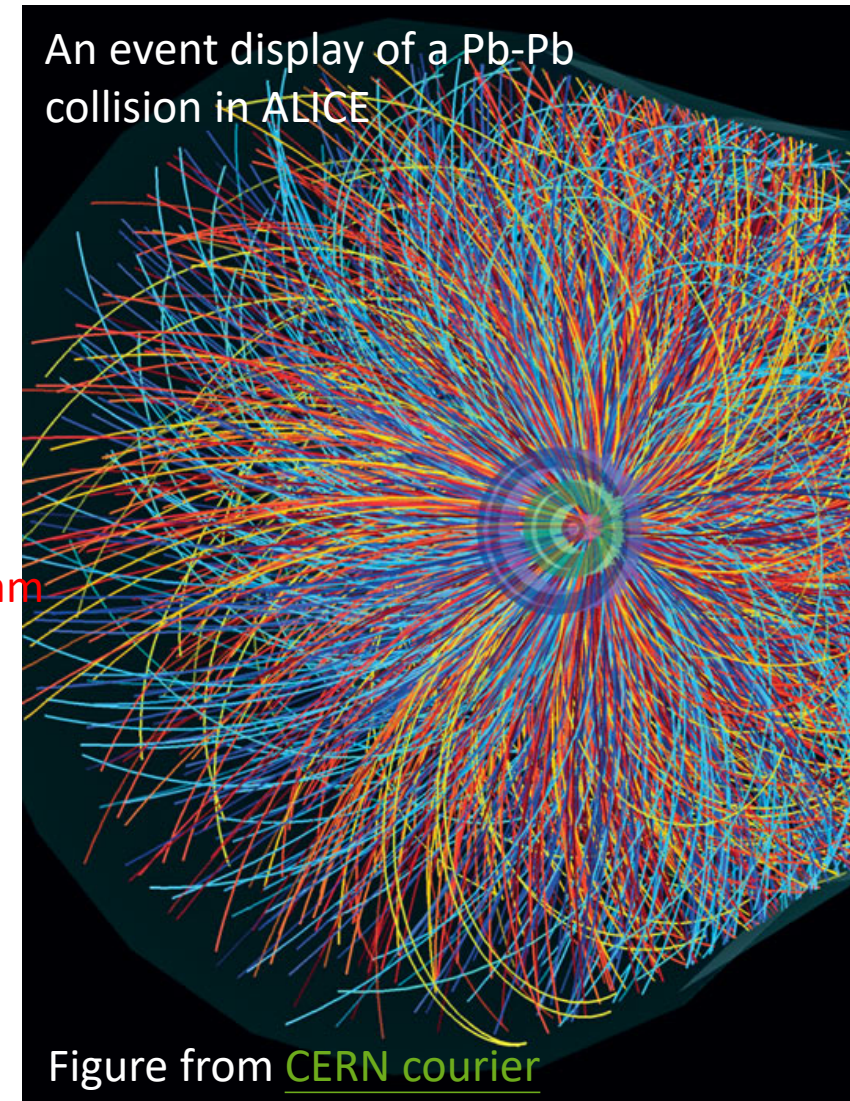
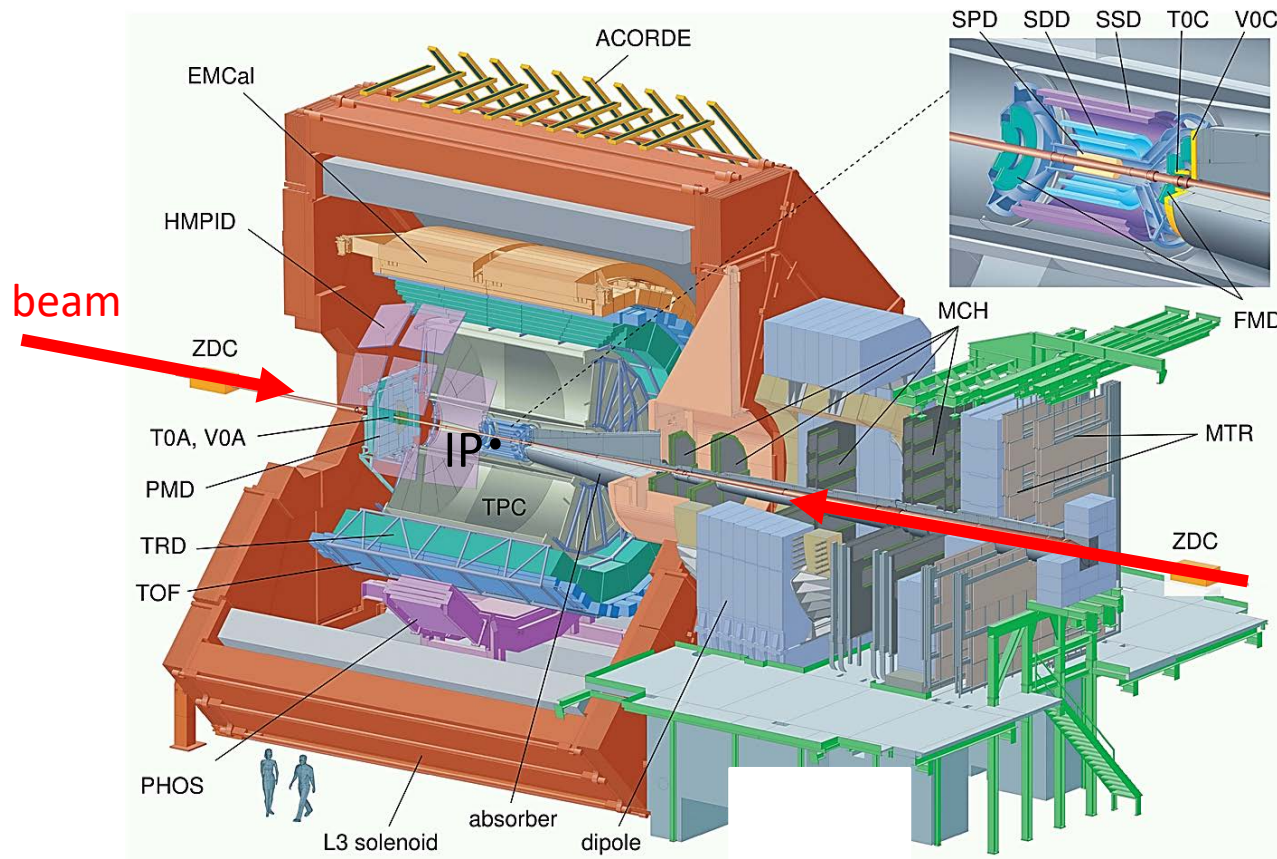


Figure from [RIKEN BNL](#)

ALICE detector and event display



The QGP in heavy-ion collisions

Maria Elena Tejeda-Yeomans, arxiv: 2004.13812 [2020]

Four stages of a heavy-ion collision and its evolution:

(a) The two heavy-ions moving towards each other



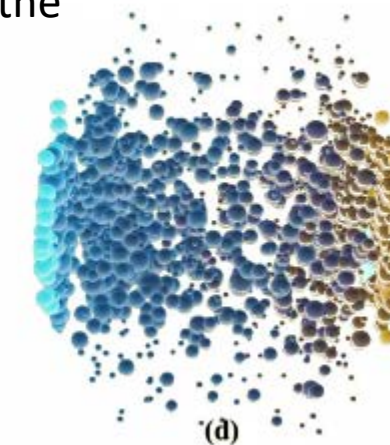
(a)



(b)



(c)



(d)

(b) The overlapping nuclei at the initial collision stage.

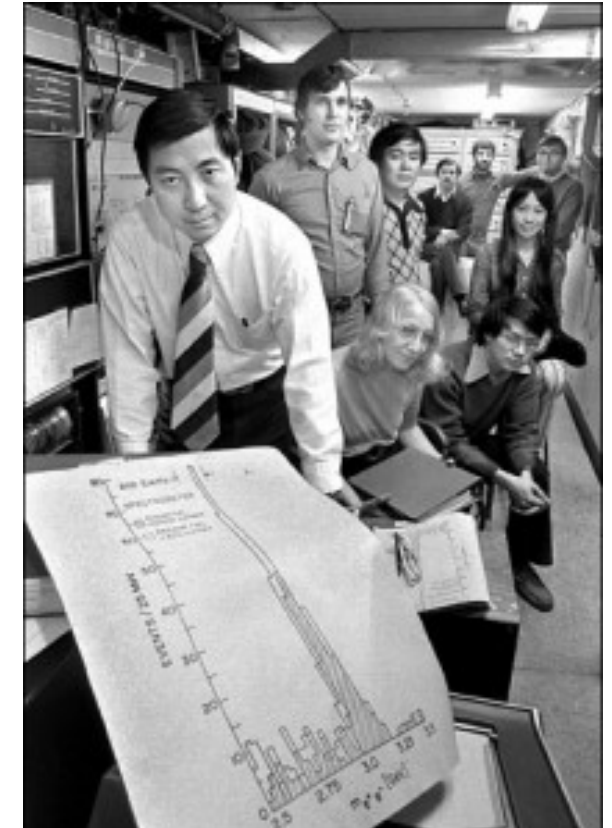
(c) At high temperature and/or high density, the QGP is created just after the collision.

(d) The system cools down and expands. The produced partons hadronize and form a hadron gas. Then the system enters chemical and kinetic freeze-out stages.

Introduction to J/ ψ particle

- In 1974, J/ ψ particles were simultaneously discovered at the Alternating Gradient Synchrotron (AGS) in Brookhaven National Laboratory (BNL) and at Stanford Positron-Electron Asymmetric Rings (SPEAR) in Stanford Linear Acceleration Center (SLAC)
- A J/ ψ particle's mass is about $3.1 \text{ GeV}/c^2$.
- A J/ ψ particle consists of a c and anti- c quarks.
- A J/ ψ particle has probability of about 5.96% to decay into a dimuon pair.

- A $c\bar{c}$ pair is produced prior to the formation of the QGP \rightarrow it experiences the full system evolution.



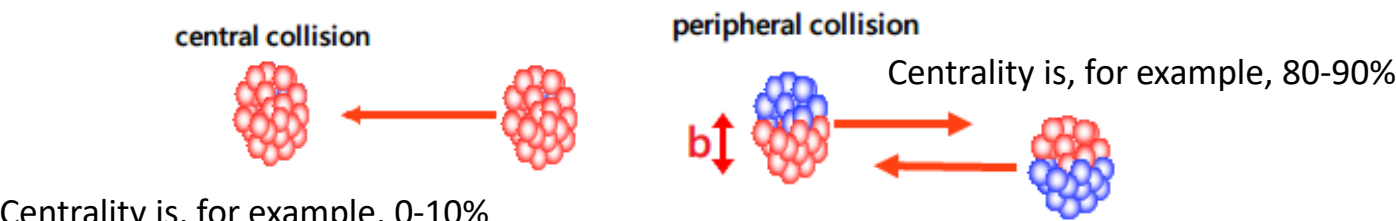
Samuel Ting and his BNL team. Credit: BNL

Collision geometry and physics quantities

$$N = L\sigma\epsilon$$

number of events observed integrated luminosity (m^{-2}) production cross section (m^2) efficiency (acceptance) ϵ : fraction of events detected

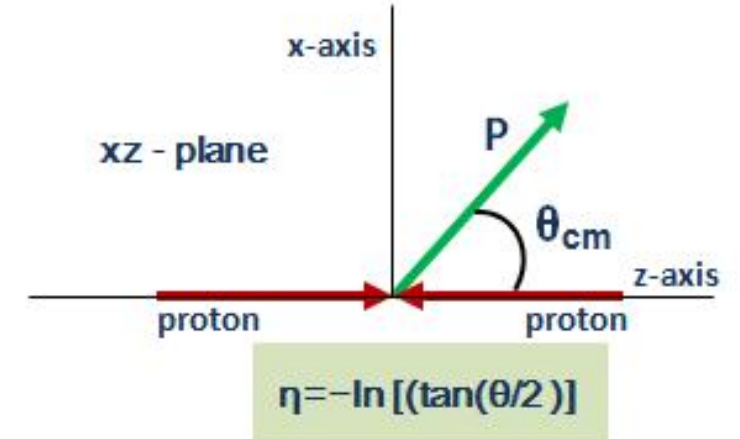
Cross section is a measurement of the probability that a process will take place.



The impact parameter \vec{b} : the distance between the center of the two nuclei in a plane transverse to the beam axis.

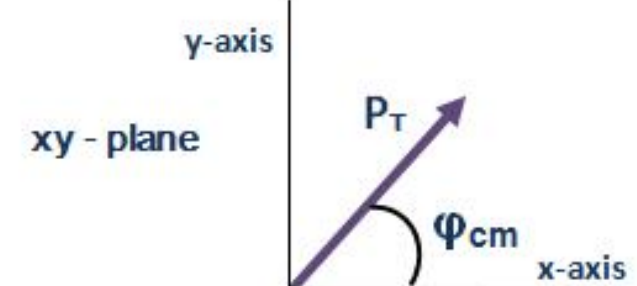
Number of participants: N_{part} . The more N_{part} is the more central collision is.

Figure from [online resources](#)



$$\eta = -\ln [(\tan(\theta/2))]$$

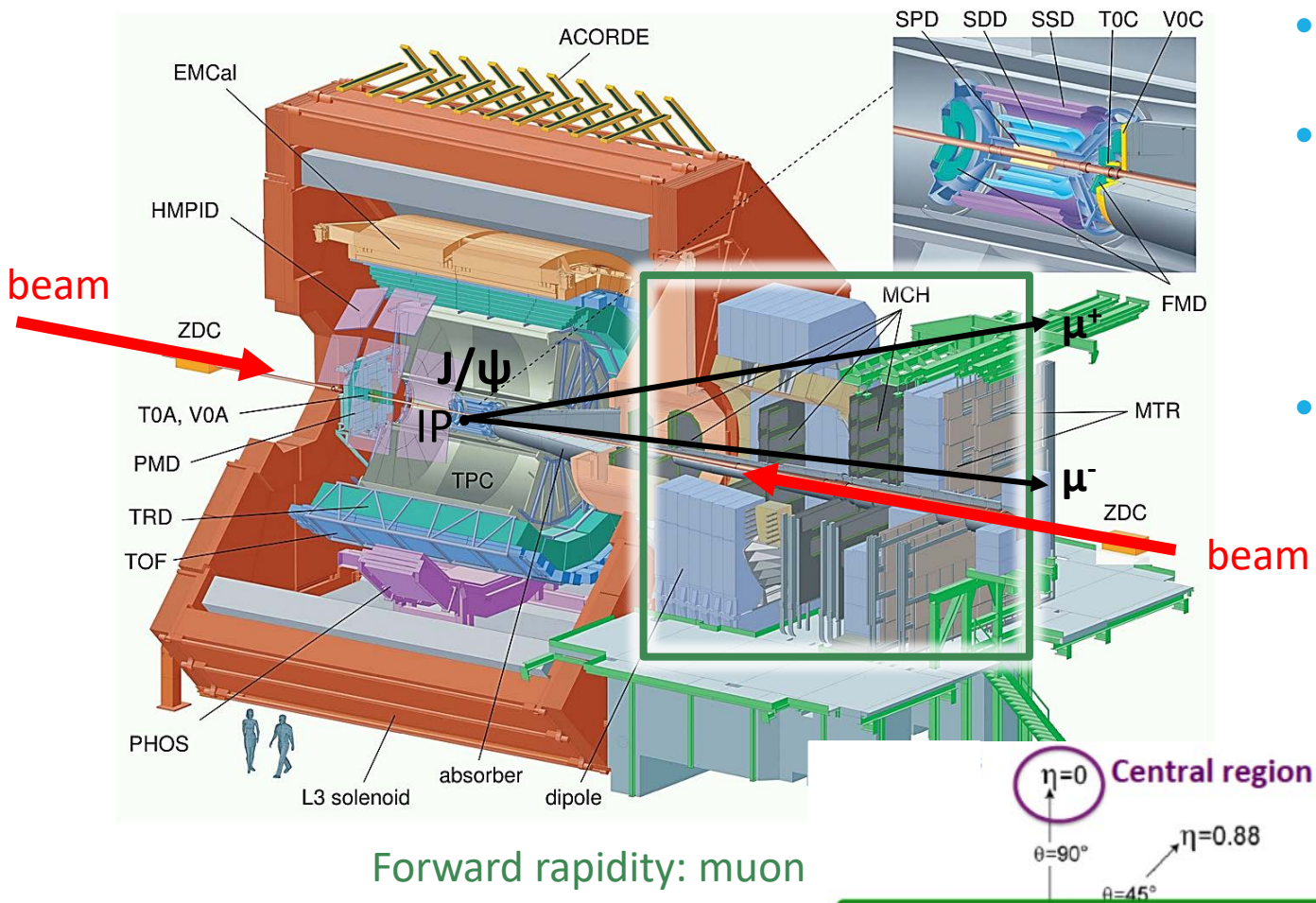
Pseudorapidity, η



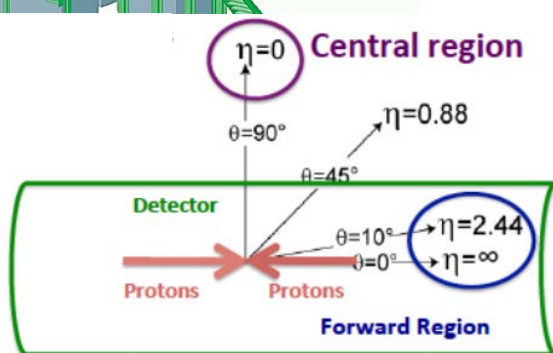
$$P_T = P \cdot \sin \Phi_{\text{cm}}$$

Transverse momentum, p_T

Measurement of J/ ψ with the ALICE detector



- Measure inclusive J/ψ production via dimuon decay in **muon spectrometer** ($2.5 < y < 4$).
- Muon spectrometer
 - **Absorber system**
 - **Tracking chambers**
 - **Dipole magnet**
 - **Trigger chambers**
- Other ALICE detectors used for muon analysis
 - SPD \rightarrow vertex; T0 \rightarrow trigger
 - V0 (V0A and V0C) \rightarrow centrality, trigger and background rejection
 - ZDC \rightarrow background rejection



Data samples and analysis tools

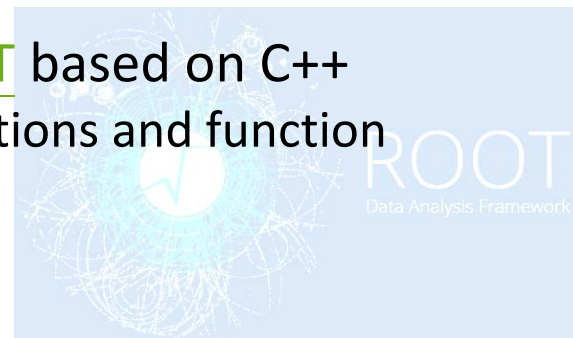
	pp 2015	pp 2017	Pb-Pb 2015	Pb-Pb 2018	
Luminosity	$\approx 106 \text{ nb}^{-1}$	$\approx 1223 \text{ nb}^{-1}$	$\approx 225 \mu\text{b}^{-1}$	$\approx 537 \mu\text{b}^{-1}$	$1\text{b} = 10^{-28} \text{ m}^2$

$$L_{\text{int}}^{2017,\text{pp}} \approx 10 \times L_{\text{int}}^{2015,\text{pp}}$$
$$L_{\text{int}}^{2018,\text{Pb--Pb}} \approx 2.4 \times L_{\text{int}}^{2015,\text{Pb--Pb}}$$

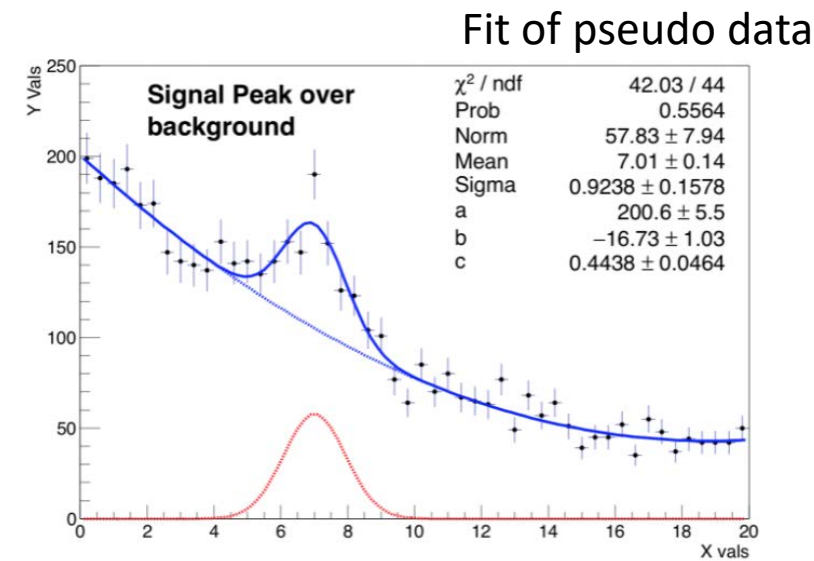
Event and track selections, dimuon selection are set to remove background events and to select the possible candidate of dimuons.

Analysis program and library used: [ROOT](#) based on C++

- histogramming and graphing for distributions and function
- fitting
- Statistics tools for data analysis
- ...



LHC computing grid was used.



Observables

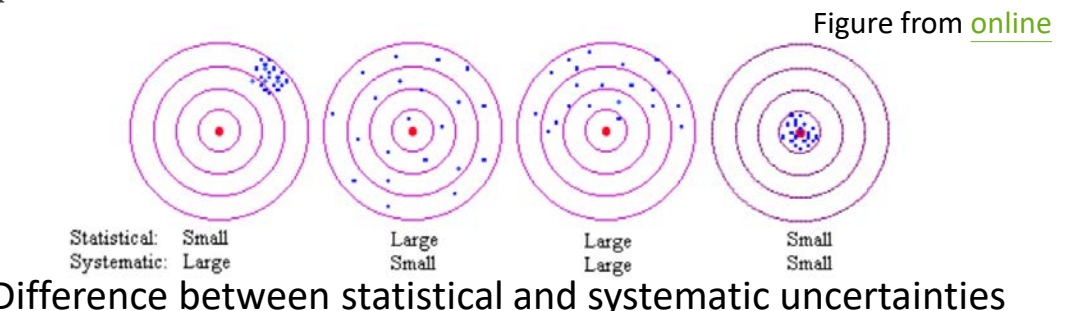
- Inclusive J/ ψ cross section σ_{pp} in pp collisions:

$$\sigma_{pp} = \frac{N_{J/\psi \rightarrow \mu\mu}}{BR(J/\psi \rightarrow \mu\mu) \cdot L_{int} \cdot A \times \epsilon}$$

- BR($J/\psi \rightarrow \mu\mu$): J/ψ to dimuon branching ratio (5.96 ± 0.03)%
 - L_{int} : integrated luminosity ($= \frac{N_{MB}}{\sigma_{MB}}$) with N_{MB} the number of minimum bias (MB) events and σ_{MB} the visible (MB) cross section at $\sqrt{s} = 5.02$ TeV.
 - $N_{J/\psi \rightarrow \mu\mu}$: number of J/ψ
 - $A \times \epsilon$: acceptance and efficiency
- Nuclear modification factor R_{AA} in heavy-ion collisions:

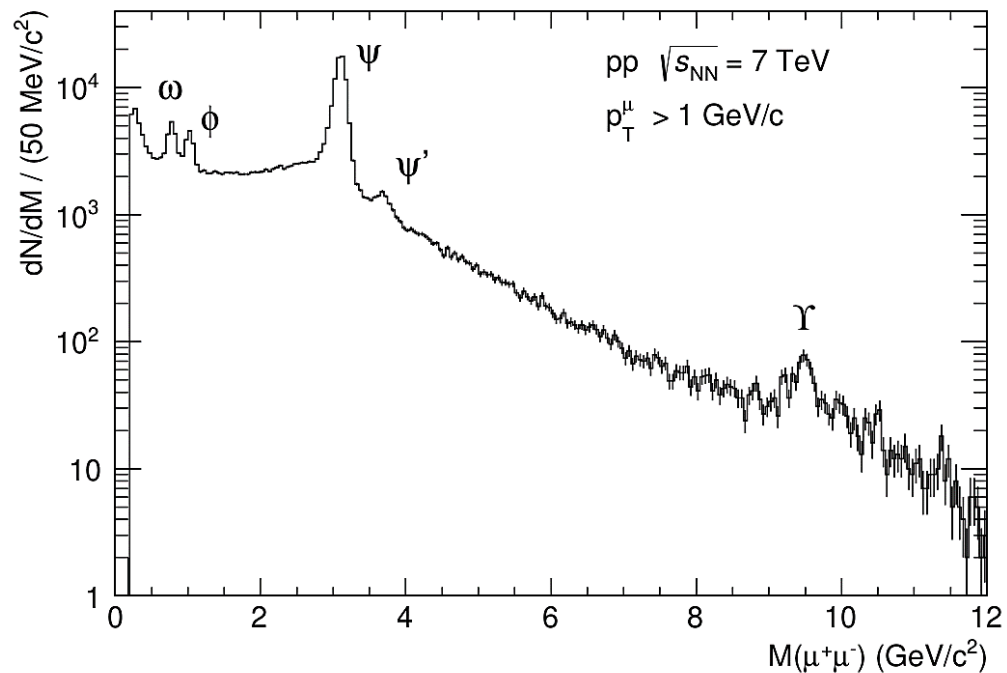
$$R_{AA} = \frac{Y_{AA}}{\langle T_{AA} \rangle \cdot \sigma_{pp}} = \frac{N_{J/\psi \rightarrow \mu\mu}}{\langle T_{AA} \rangle \cdot \sigma_{pp} \cdot BR(J/\psi \rightarrow \mu\mu) \cdot N_{MB} \cdot A \times \epsilon}$$

- Y_{AA} : J/ψ invariant yield
- $\langle T_{AA} \rangle$: average nuclear overlap function



J/ψ signal extraction

- Signal events:
 - Fully correlated dimuons decayed from J/ψ produced directly from collisions.
- Background events:
 - Uncorrelated dimuons coming from different physics processes: $K \rightarrow \mu + X$; $\pi \rightarrow \mu + X$
- These two types of events populate the invariant-mass spectra.



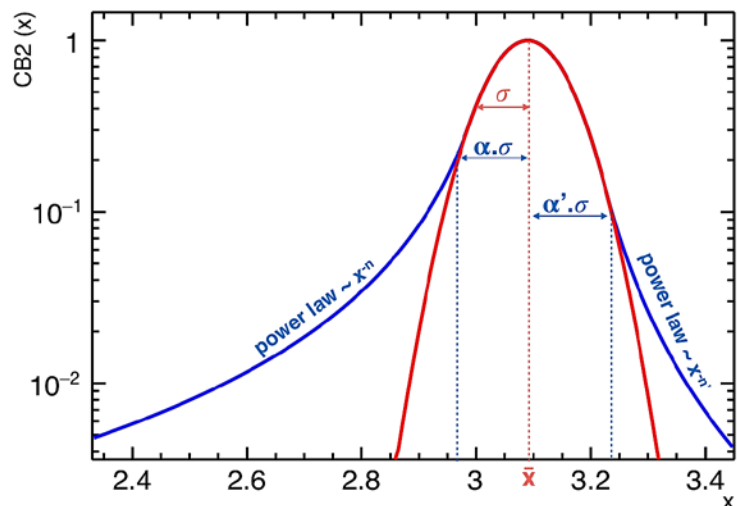
Invariant mass, M , for dimuon:

$$M_{\mu^+\mu^-} = \sqrt{m_{\mu^+}^2 + m_{\mu^-}^2 + 2(E_{\mu^+}E_{\mu^-} - \mathbf{p}_{\mu^+} \cdot \mathbf{p}_{\mu^-})}$$

J/ψ signal extraction and fit functions

- In order to extract the J/ψ signal and its systematic uncertainty, various fitting functions are adopted:
 - Signal functions
 - Background functions
- In addition, two fitting ranges in invariant mass are used.

An example of a signle function, extended Crystal Ball (CB)



\bar{x} : mean

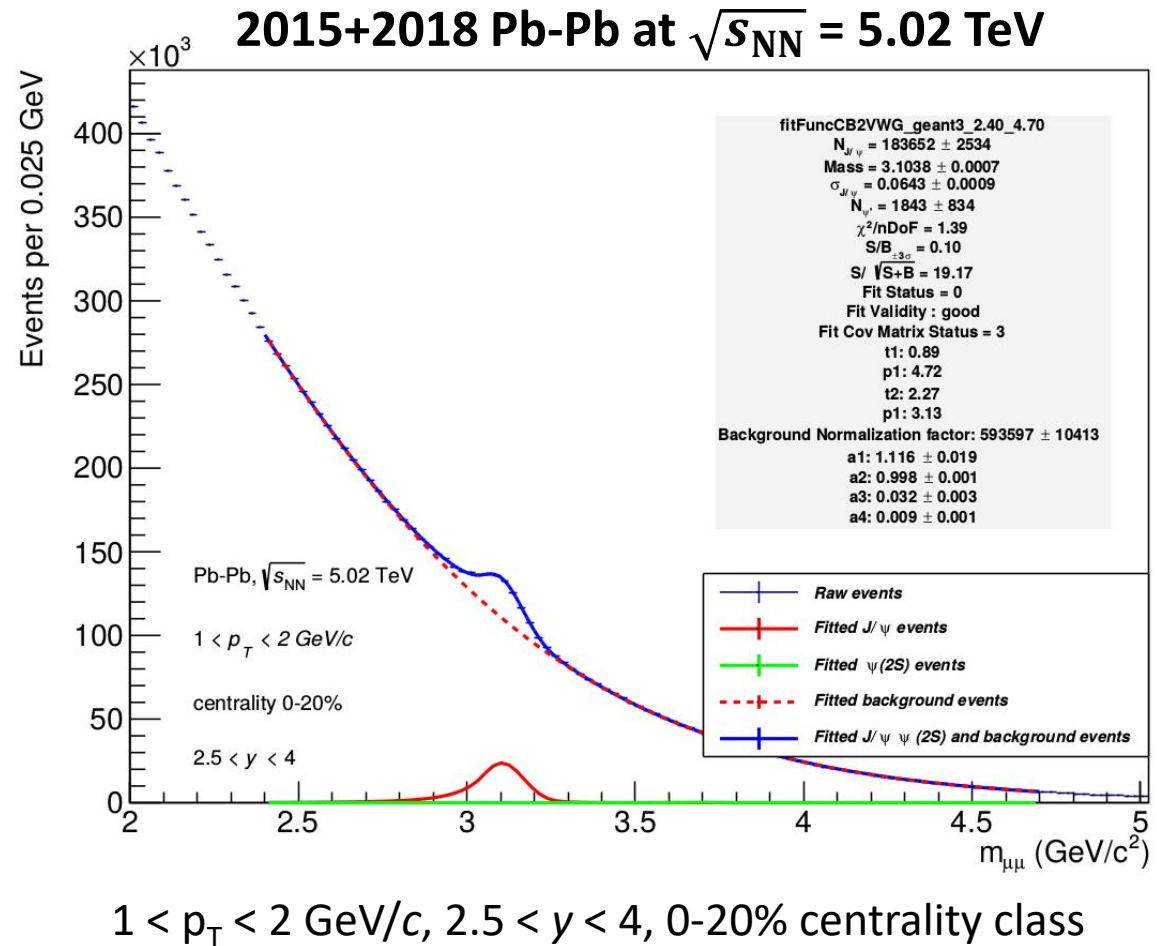
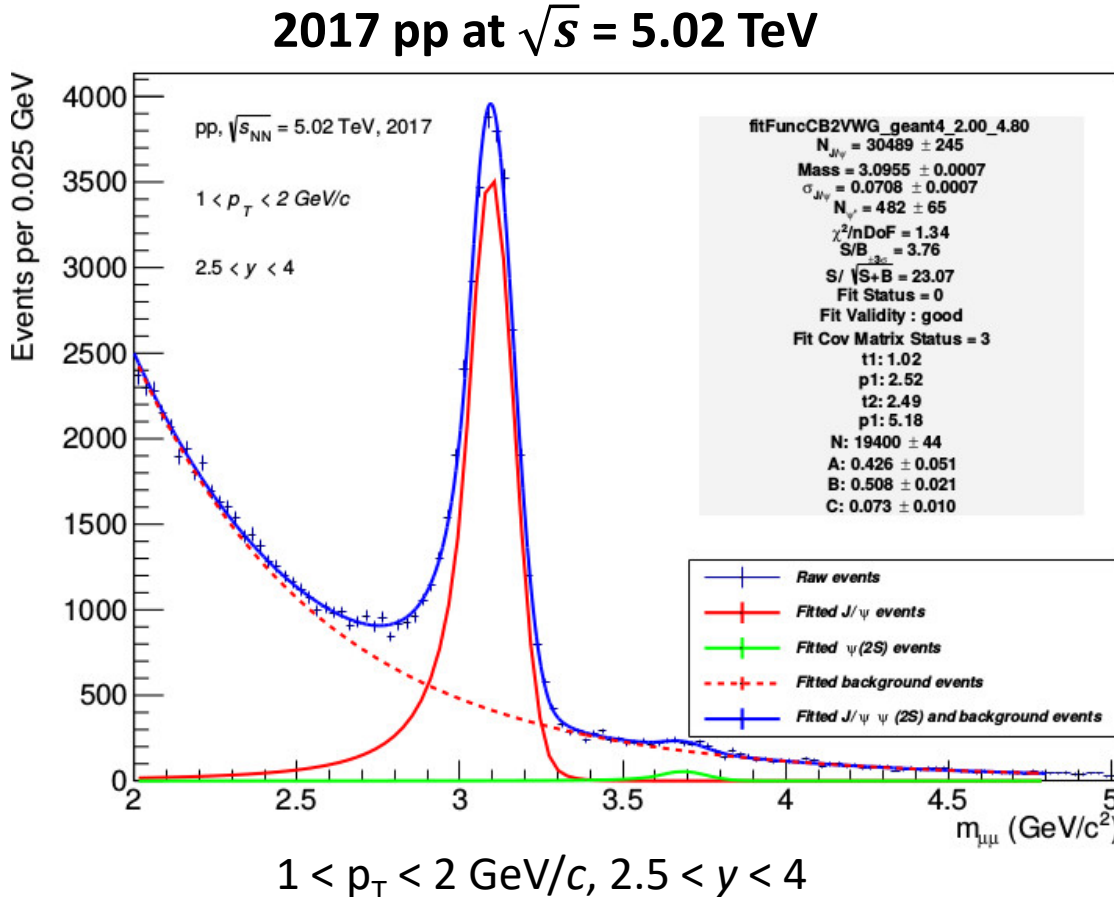
σ : width

(α, n, α', n') : 4 tail parameters fixed to MC simulation and from free tails fit to large statistics pp data sample (integrated over p_T and y).

In addition, for NA60 function, 8 tail parameters are fixed to MC simulation.

$$f(x) = N \cdot \begin{cases} A \cdot \left(B - \frac{x - \bar{x}}{\sigma} \right)^{-n}, & \frac{x - \bar{x}}{\sigma} < -\alpha \\ \exp\left(-\frac{(x - \bar{x})^2}{2\sigma^2}\right), & -\alpha \leq \frac{x - \bar{x}}{\sigma} < \alpha' \\ C \cdot \left(D + \frac{x - \bar{x}}{\sigma} \right)^{-n'}, & \frac{x - \bar{x}}{\sigma} \geq \alpha' \end{cases}$$

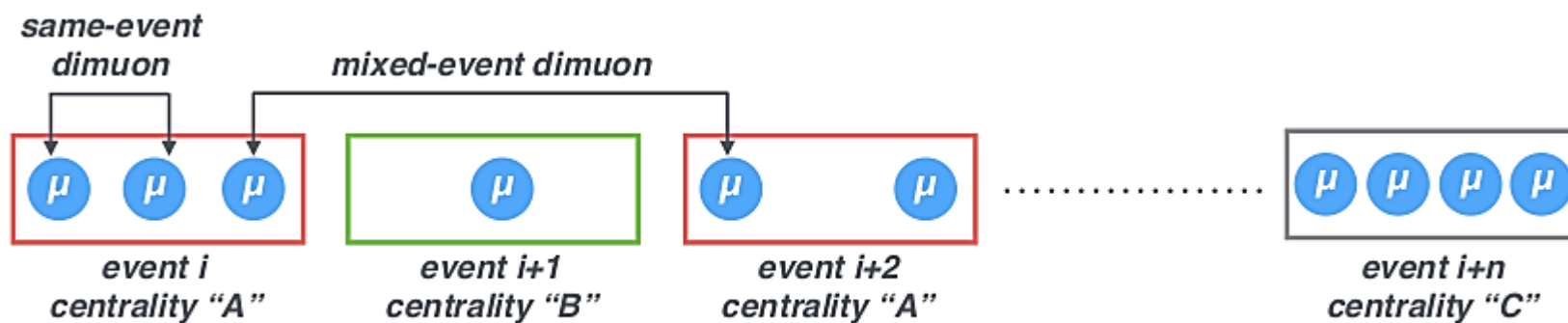
J/ ψ signal extraction in pp and Pb-Pb



- Fitting uses the log likelihood method.
- Integral of function in bin is used, instead of value at bin center.

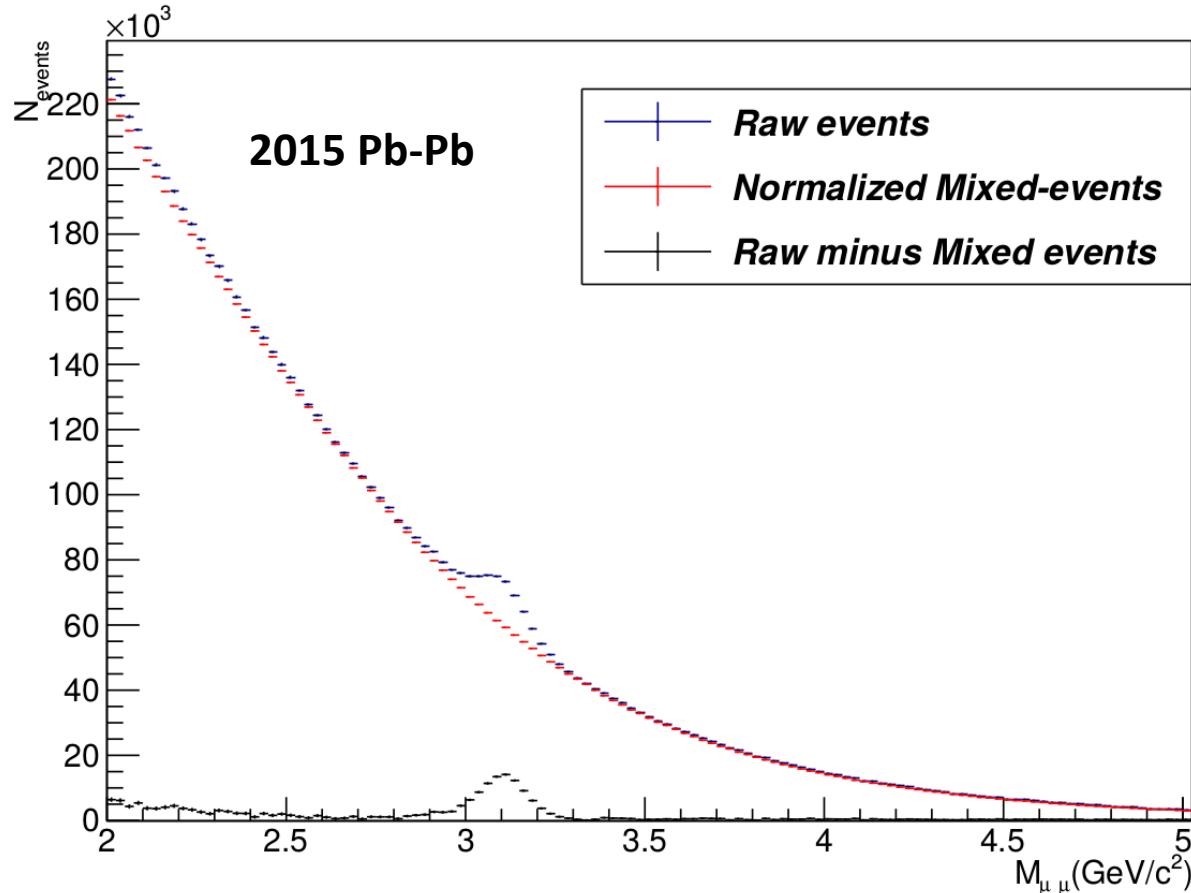
J/ ψ signal extraction in Pb-Pb: event mixing (1)

- Event mixing method estimates the background events which is **uncorrelated dimuons** coming from different physics process: $K \rightarrow \mu + X; \pi \rightarrow \mu + X$
- Subtraction of the uncorrelated dimuon events from real data

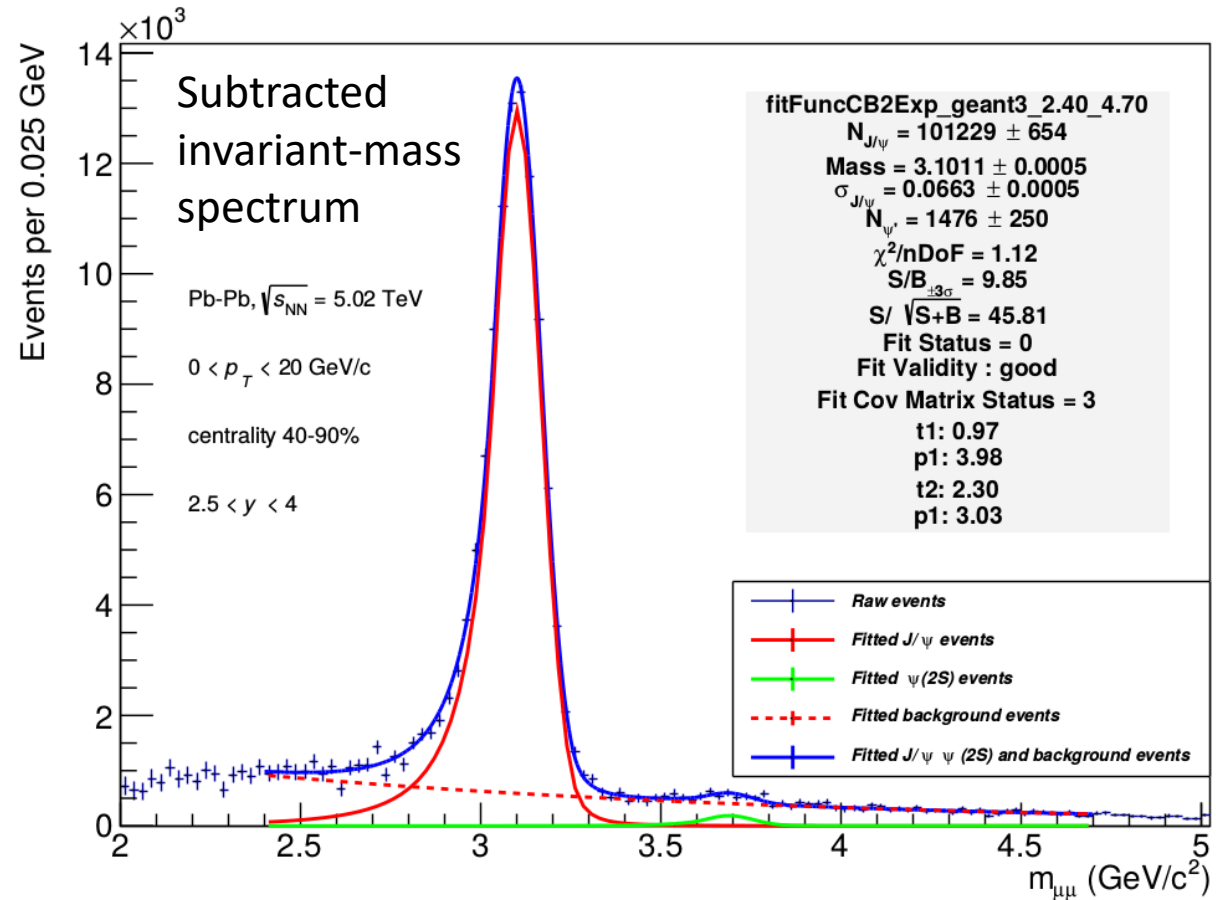


- Pools are created and save the events sharing similar global properties, such as centrality.
- In a pool, each muon particle combines all the other muon particle from the 20 events.

J/ ψ signal extraction in Pb-Pb: event mixing (2)



Event mixing technique used to describe the uncorrelated background by mixing muons from different events



- Fitting uses the least square method.
- Integral of function in bin is used, instead of value at bin center.

Acceptance and efficiency

- The J/ ψ detection is affected by the acceptance and efficiency, $A \times \epsilon$, of the detector during data taking.
- MonteCarlo (MC) simulations are used to estimate $A \times \epsilon$.
 - Event generator generating J/ ψ according to input p_T and y distributions which are given by

$$\bullet \quad f(p_T) = p_0 \times \frac{p_T}{\left[1 + \left(\frac{p_T}{p_1}\right)^{p_2}\right]^{p_3}} \text{ and } f(y) = p_4 \times \exp^{-0.5\left(\frac{y}{p_5}\right)^2} \text{ where } p_{0-5} \text{ are free parameters.}$$

- From MC production, acceptance and efficiency, $A \times \epsilon (\Delta p_T)$, is defined as

$$A \times \epsilon (\Delta p_T) = \frac{N_{J/\Psi}^{\text{rec.}}(\Delta p_T^{\text{rec.}})}{N_{J/\Psi}^{\text{gen.}}(\Delta p_T^{\text{gen.}})} \quad \begin{cases} N_{J/\Psi}^{\text{rec.}}, \text{number of reconstructed J}/\psi \\ N_{J/\Psi}^{\text{gen.}}, \text{number of generated J}/\psi \end{cases}$$

- Its uncertainty is computed by selecting maximum between $1/N_{\text{gen.}}$ and binomial error $\sigma_{\text{bino.}}$ which is defined by

$$\bullet \quad \sigma_{\text{bino.}} = \sqrt{\frac{N_{\text{rec.}}}{N_{\text{gen.}}} \times \left(\frac{1 - N_{\text{rec.}}/N_{\text{gen.}}}{N_{\text{gen.}}} \right)}, \text{ if } N_{J/\Psi}^{\text{gen.}} \leq N_{J/\Psi}^{\text{rec.}}$$

Realistic input MC distribution: iterative procedure

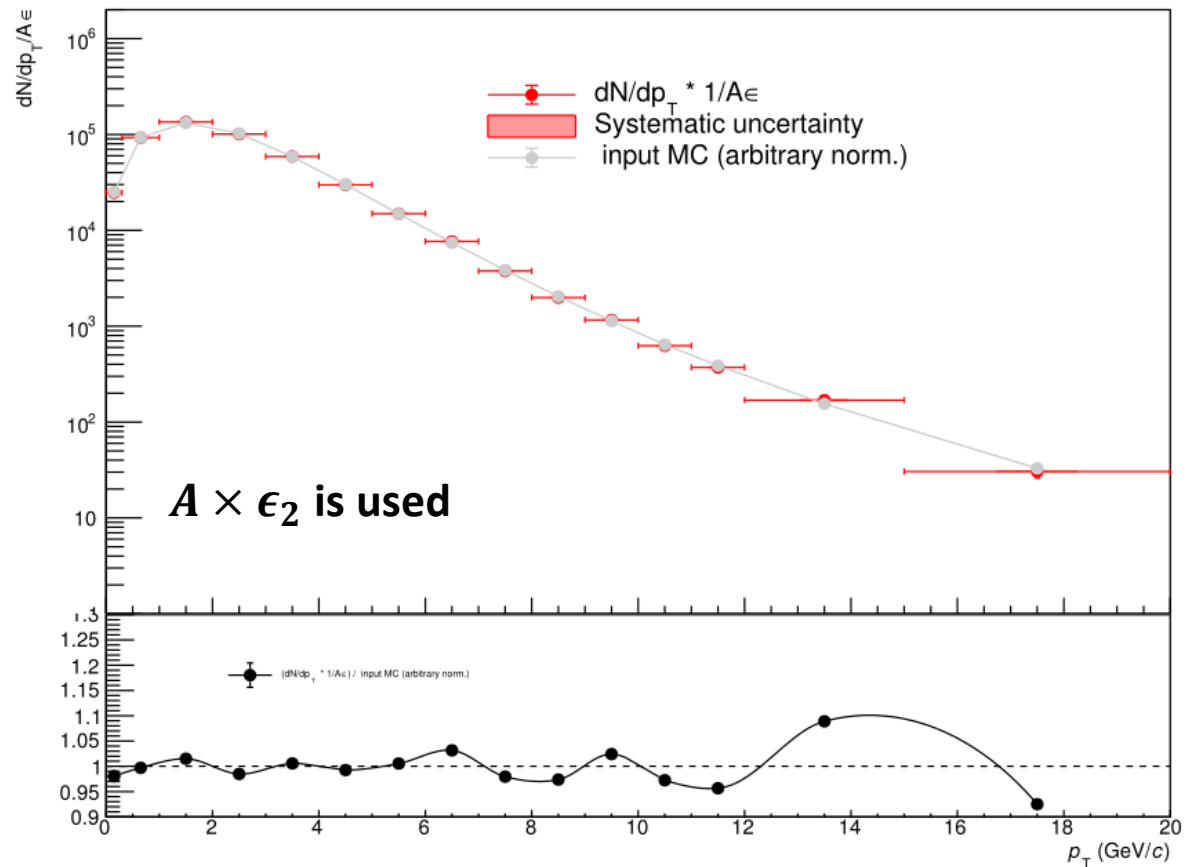
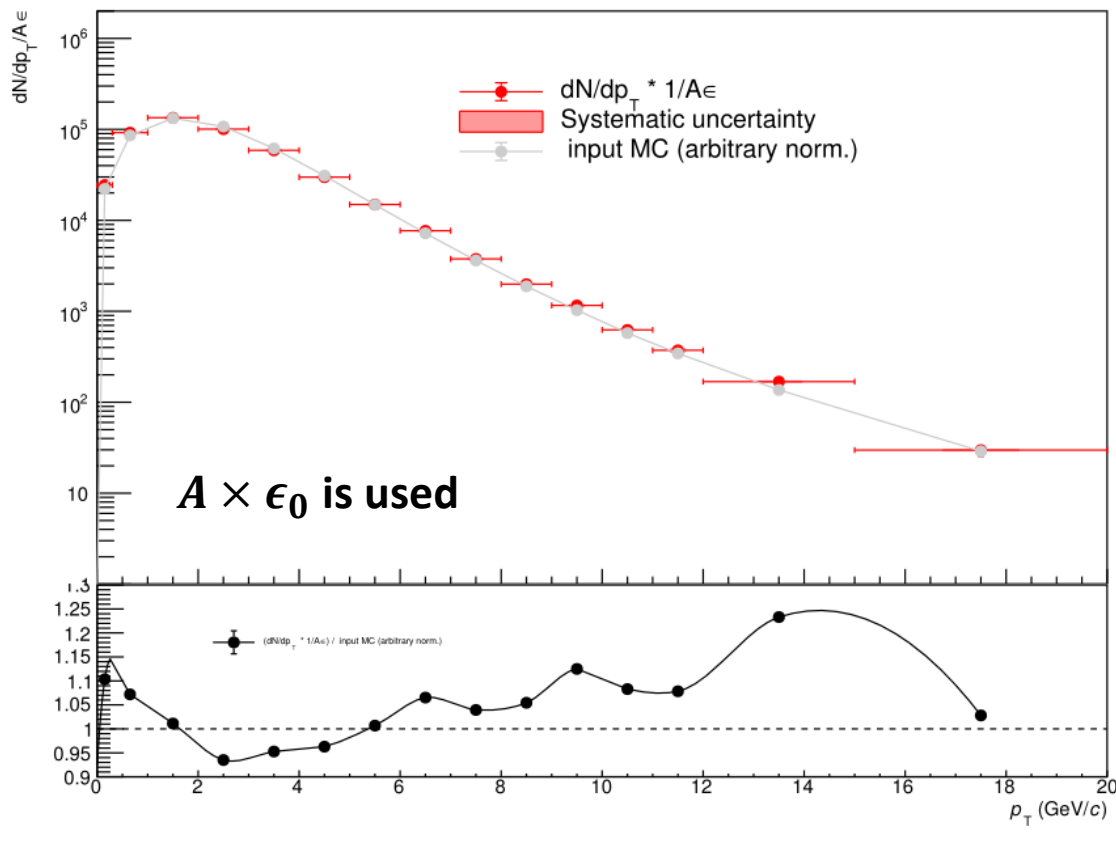
- The input distributions are tuned to the raw data corrected by $A \times \epsilon \rightarrow$ perform iterative procedure
- At step 0 of the procedure, $A \times \epsilon_0$ is first calculated with original input shape.
 - Apply a weight, $w_n(p_T^{\text{gen.}}, y^{\text{gen.}}) = w_n(p_T^{\text{gen.}}) \times w_n(y^{\text{gen.}})$, to each J/ ψ event in MC.

$$w_n(p_T^{\text{gen.}}) = \frac{f_{n-1}^{\text{corr.}}(p_T)}{f_{n-1}^{\text{gen.}}(p_T^{\text{gen.}})} \text{ and } w_n(y^{\text{gen.}}) = \frac{f_{n-1}^{\text{corr.}}(y)}{f_{n-1}^{\text{gen.}}(y^{\text{gen.}})}$$

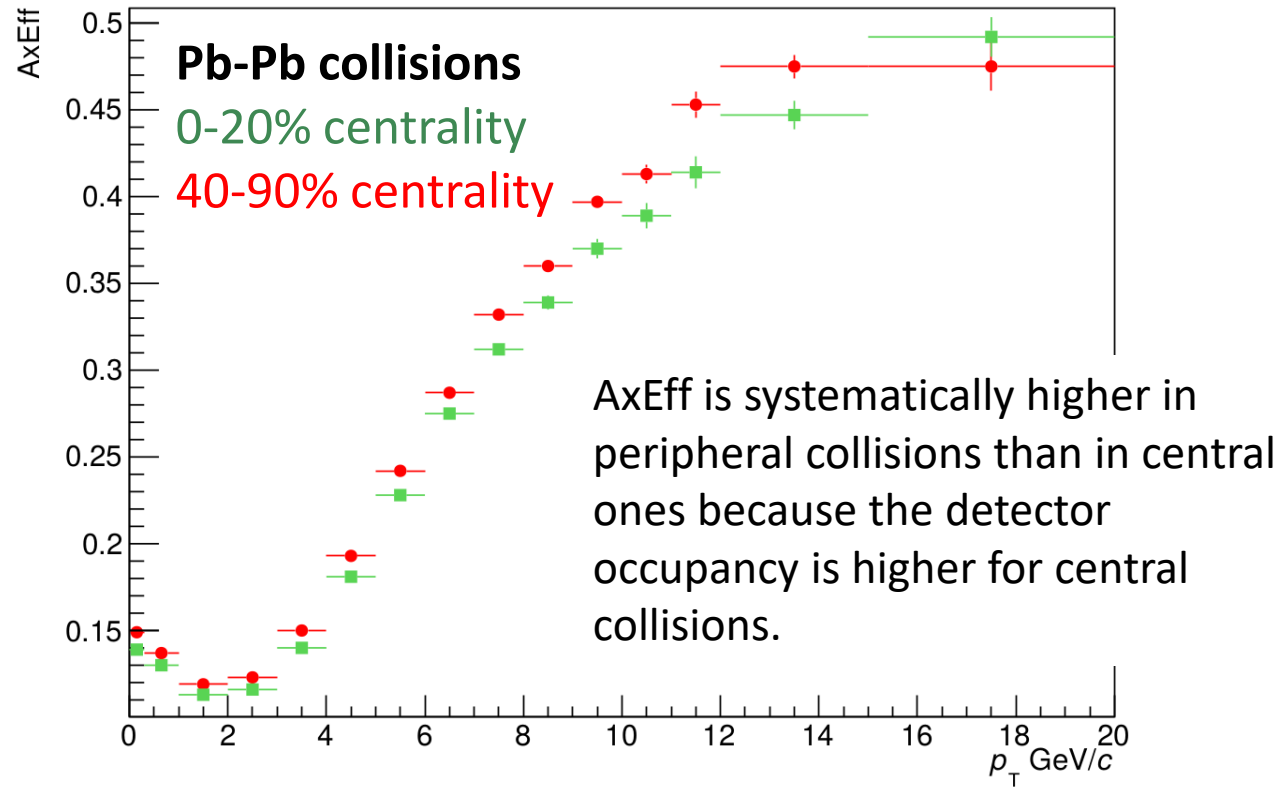
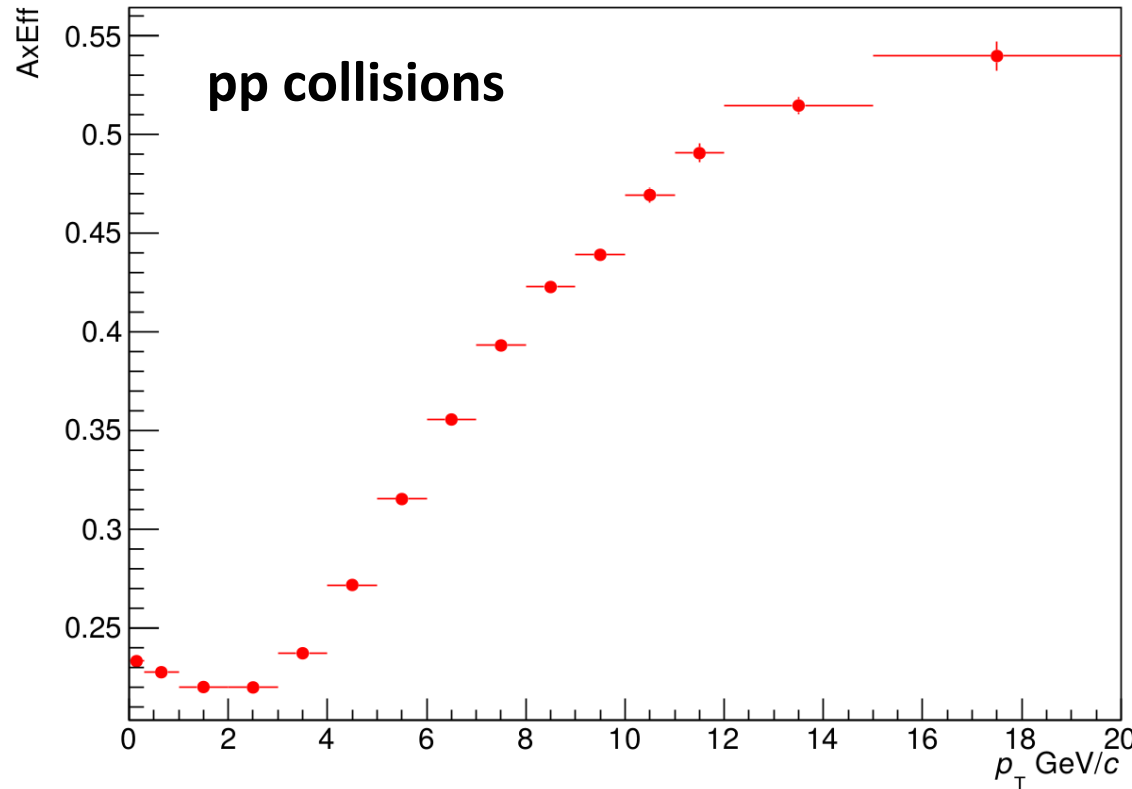
- Corrected input shapes, $f_{n-1}^{\text{corr.}}(p_T)$ and $f_{n-1}^{\text{corr.}}(y)$, parameters are obtained by fitting in the raw yield, raw data corrected by $A \times \epsilon$.

Realistic input MC distribution: iterative procedure

- The input distributions are tuned to the raw data corrected by $A \times \epsilon \rightarrow$ perform iterative procedure
- At step 0 of the procedure, $A \times \epsilon_0$ is first calculated with original input shape.
 - Apply a weight, $w_n(p_T^{\text{gen.}}, y^{\text{gen.}}) = w_n(p_T^{\text{gen.}}) \times w_n(y^{\text{gen.}})$, to each J/ ψ event in MC.



Acceptance and efficiency



- MC signal is embedded into real events in Pb-Pb in order to reproduce the detector inefficiency for high-multiplicity events.

Systematic uncertainties

Systematic uncertainties in experimental observations usually come from the measuring instruments

- **pp analysis:**
 - Branching ratio
 - Luminosity
 - Signal extraction
 - MC input
 - Muon tracking, muon trigger and matching efficiencies
- **Pb-Pb analysis:**
 - Branching ratio
 - Normalization factor
 - Signal extraction
 - MC input
 - Muon tracking, muon trigger and matching efficiencies
 - $\langle T_{AA} \rangle$ and centrality limit
 - pp cross section

Systematic uncertainty on signal extraction

- Average number of J/ψ , $\langle N_{J/\psi} \rangle$

$$= \frac{\sum_{i=0}^{N_{\text{test}}} w_i N_{i,J/\psi}}{\sum_{i=0}^{N_{\text{test}}} w_i}$$

- Statistical uncertainties of all the

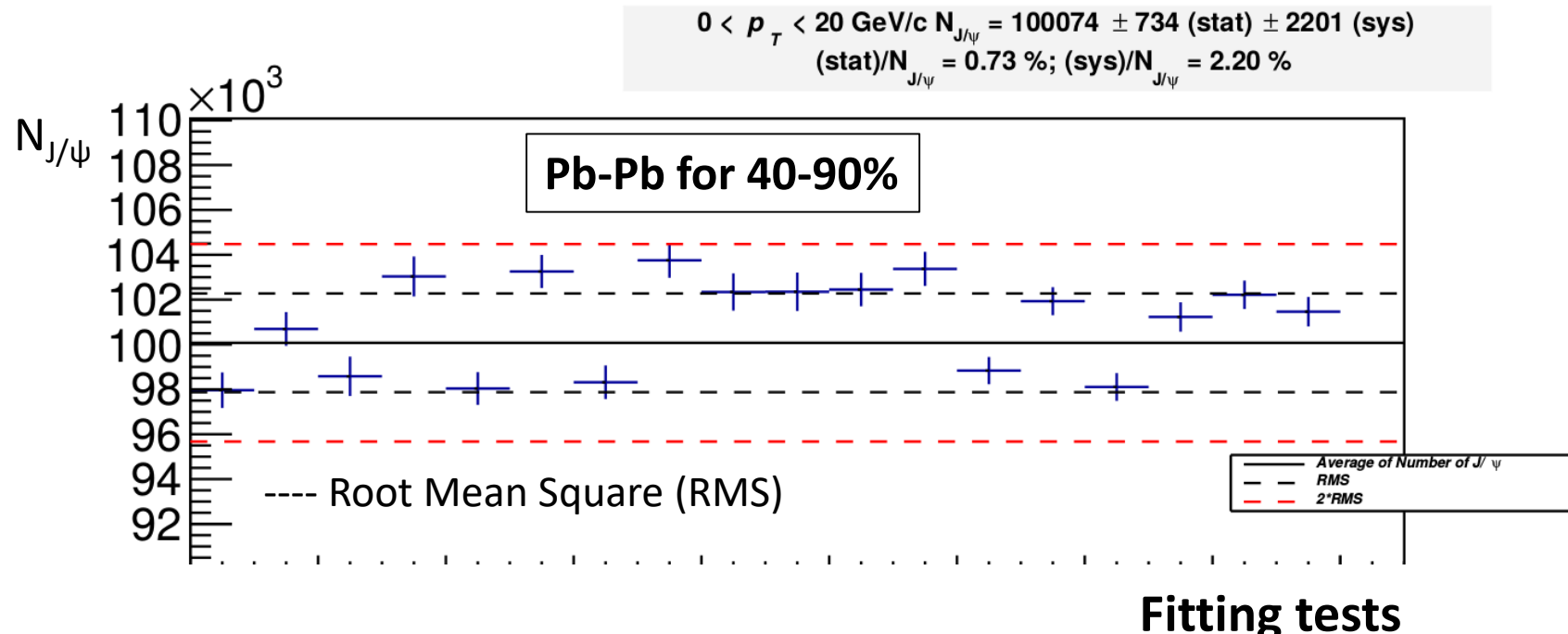
$$\text{tests}, \sigma_{N_{J/\psi}}^{\text{stat.}} = \frac{\sum_{i=0}^{N_{\text{test}}} w_i \sigma_{i,J/\psi}^{\text{stat.}}}{\sum_{i=0}^{N_{\text{test}}} w_i}$$

- Systematic uncertainty on signal

$$\text{extraction}, \sigma_{N_{J/\psi}}^{\text{syst.}} =$$

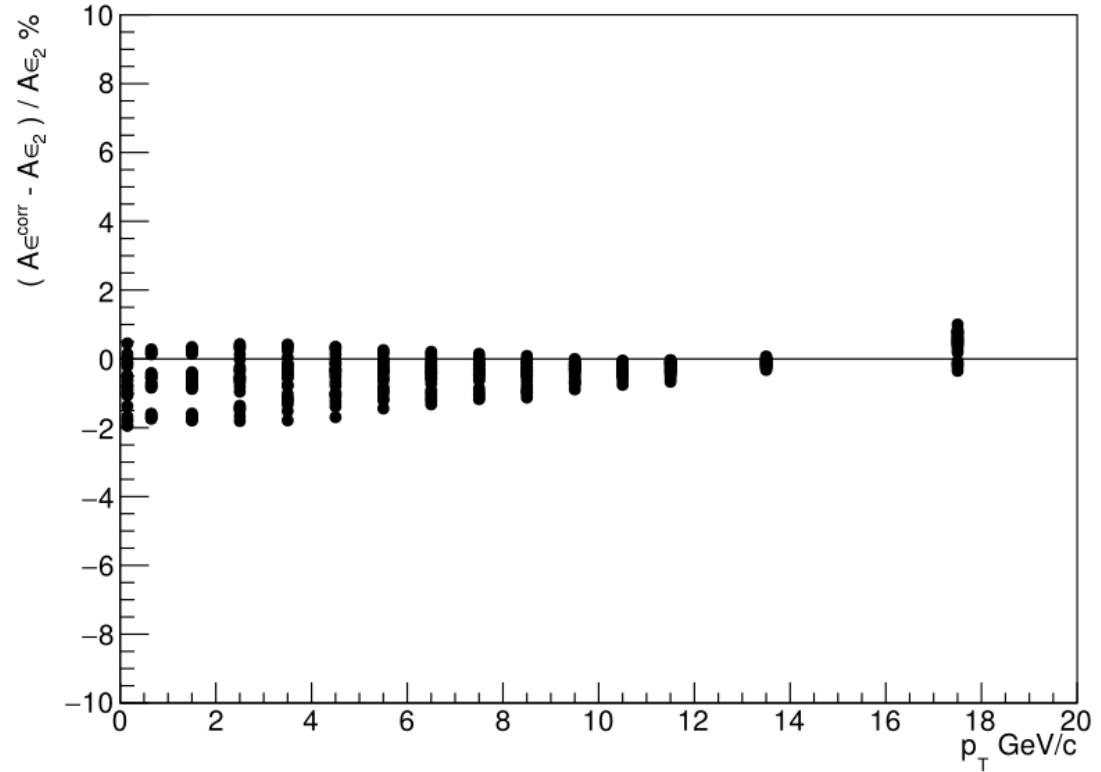
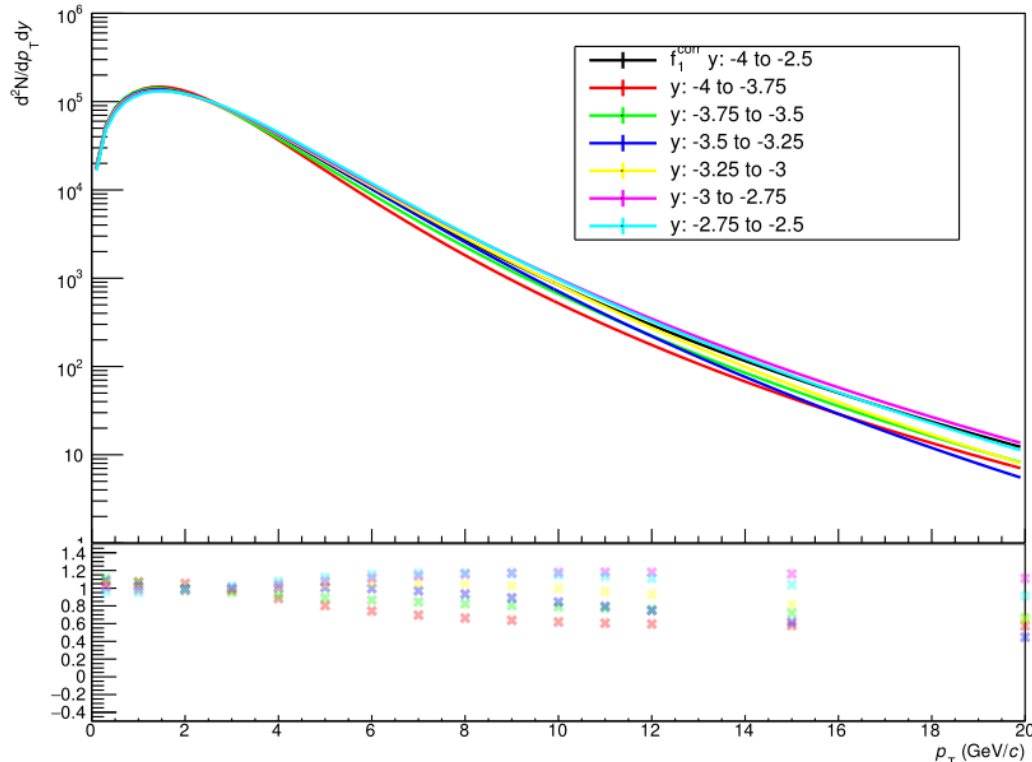
$$\sqrt{\frac{\sum_{i=0}^{N_{\text{test}}} w_i N_{i,J/\psi}^2}{\sum_{i=0}^{N_{\text{test}}} w_i} - \langle N_{J/\psi} \rangle^2}$$

$N_{i,J/\psi}$ is the raw number of J/ψ extracted from fit test i , weight w_i for a given i , the total number of tests, N_{test}



- Weights balance the fits with MC tails than the data tail
- The systematic uncertainty on signal extraction is estimated by using different fitting tests.

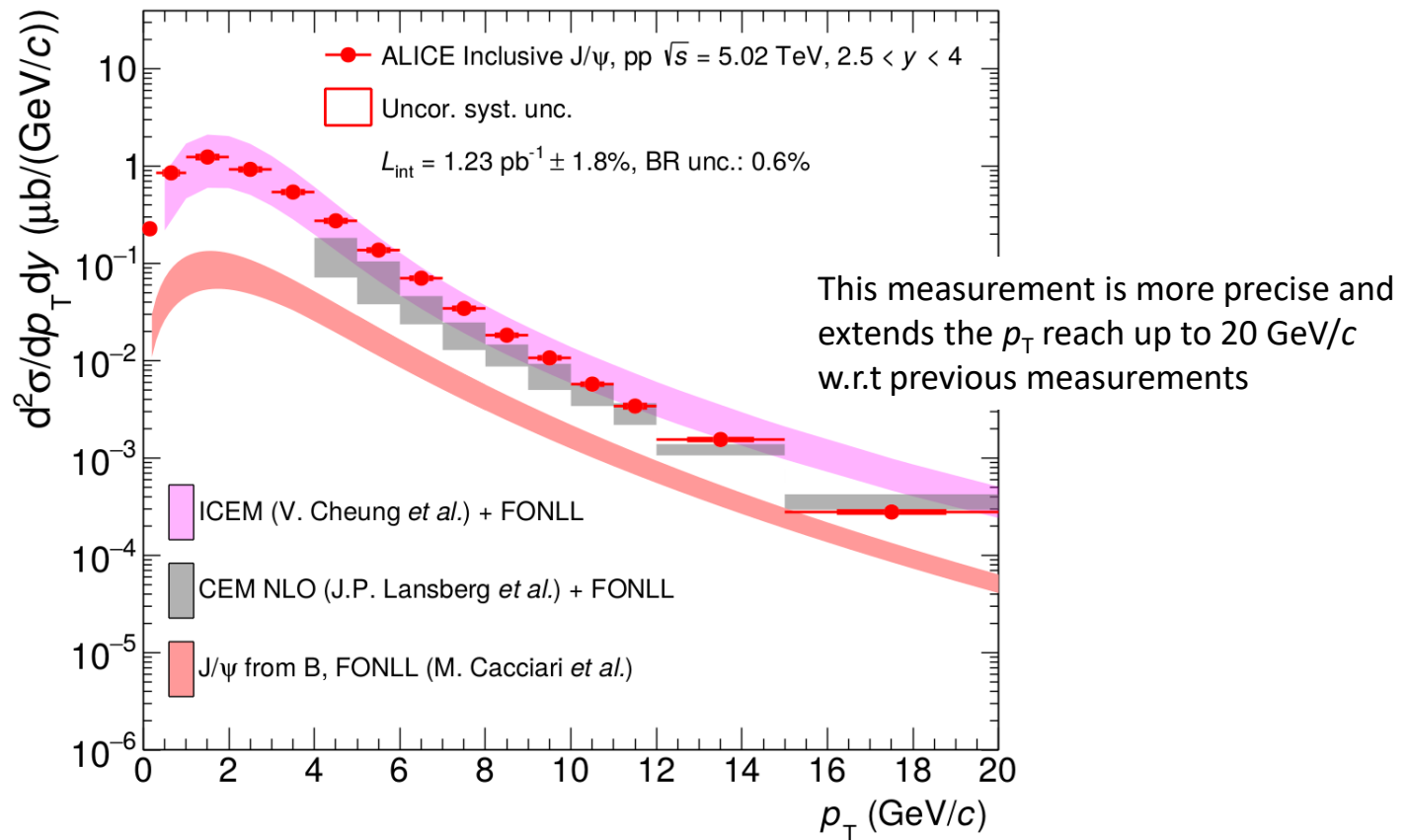
Systematic uncertainty on input J/ ψ p_T or y distribution in the MC (used for AxEff determination)



- The systematic uncertainty on input MC is dominated by the missing correlations between the p_T and y J/ ψ input shapes in the MC.
- 24 ($= 6 \times 4$) input shapes are used to calculate the syst. uncertainty on AxEff.

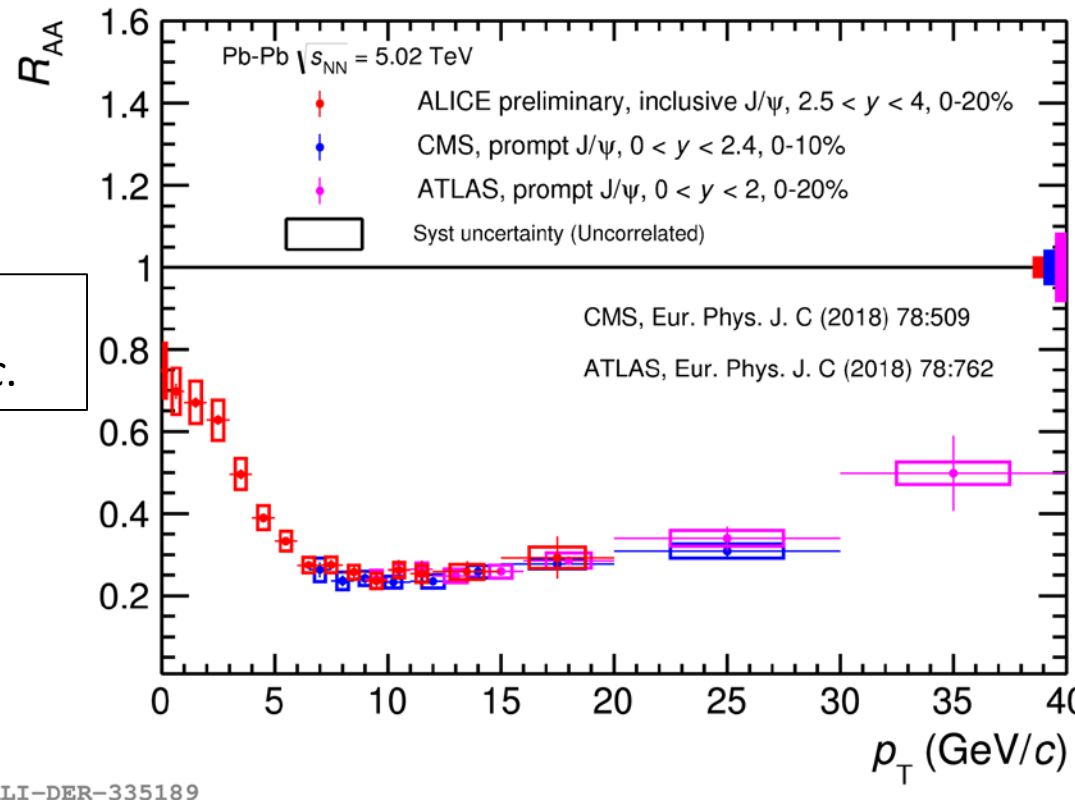
J/ ψ production in pp as a function of p_T (1)

$$\sigma_{J/\psi} = 5.877 \pm 0.03 \text{ (stat.)} \pm 0.34 \text{ (syst.) } \mu\text{b} \text{ for } p_T < 20 \text{ GeV}/c.$$



- Improved CEM describes well the data over p_T .
- CEM NLO calculation underestimates the data for $4 < p_T < 10$ GeV/c and is compatible with the data for $p_T > 10$ GeV/c.

$\text{J}/\psi R_{\text{AA}}$ as a function of p_{T} in Pb-Pb (1)



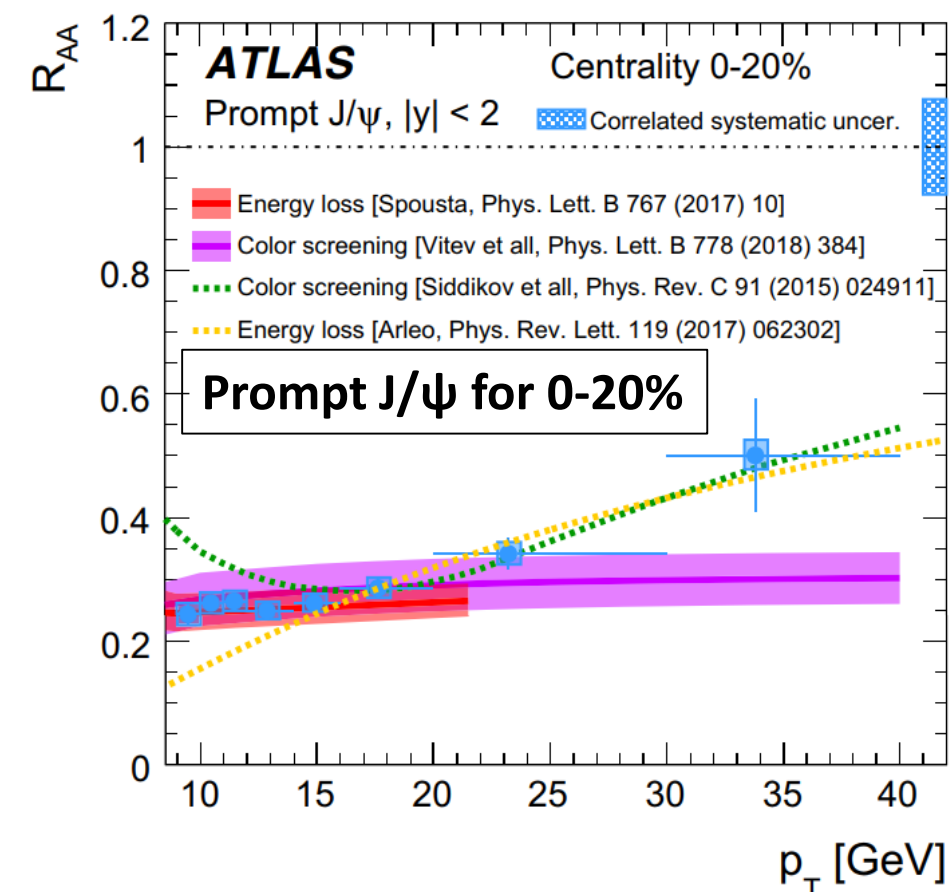
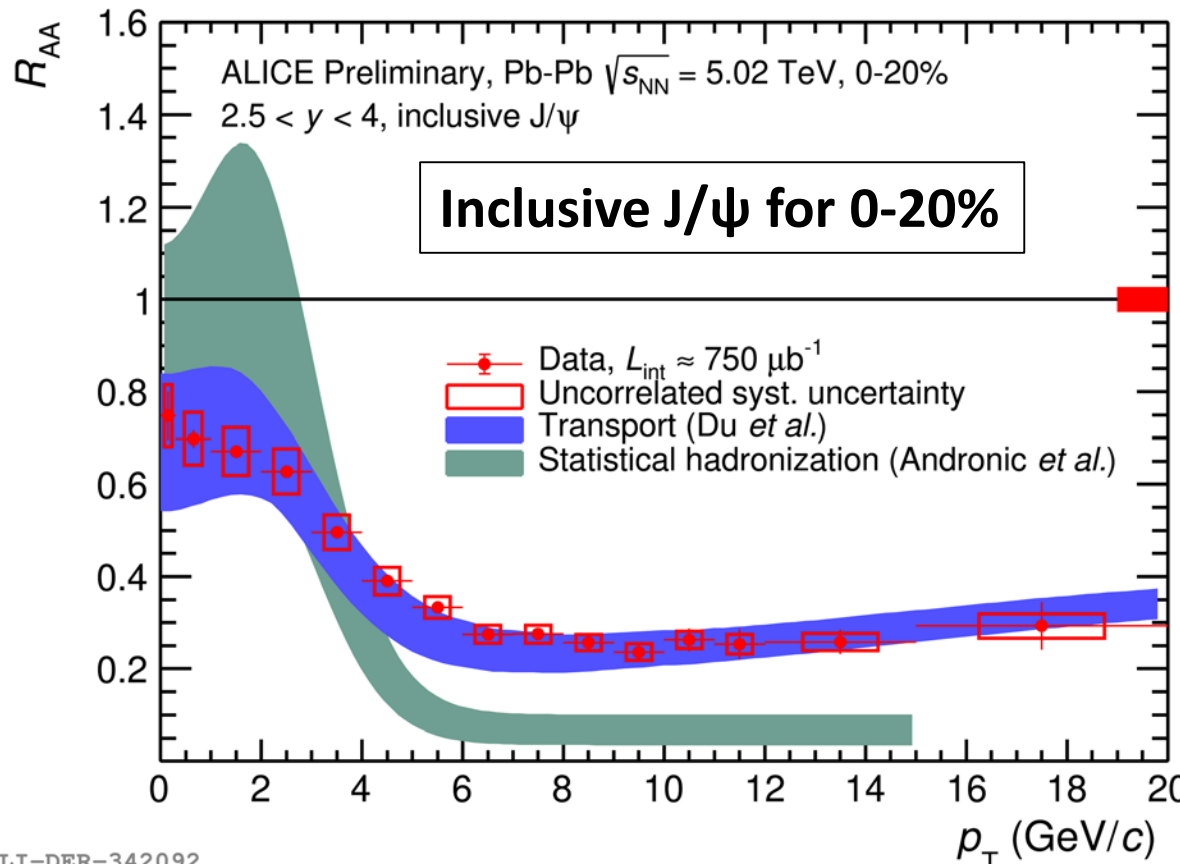
The **ALICE R_{AA}** increases with decreasing p_{T} for $p_{\text{T}} < 6 \text{ GeV}/c$.

The **ALICE R_{AA}** stays constant about 0.3 for $6 \leq p_{\text{T}} < 20 \text{ GeV}/c$.

New ALICE measurement on inclusive $\text{J}/\psi R_{\text{AA}}$. p_{T} reach up to 20 GeV/c in most central collisions.

- Good agreement of **ALICE** data with **ATLAS** and **CMS** in the common p_{T} range despite different rapidity regions.

$\text{J}/\psi R_{\text{AA}}$ as a function of p_{T} in Pb-Pb (2)



- The TM calculation reproduces the ALICE data in the full p_{T} range. The SHM calculation is compatible with the ALICE data for $p_{\text{T}} < 5 \text{ GeV}/c$ and underestimates the ALICE data for $p_{\text{T}} \geq 5 \text{ GeV}/c$.
- The calculations based on energy loss (F. Arleo) models can describe the ATLAS data for $p_{\text{T}} > 15 \text{ GeV}/c$.

ELI Beamlines

Extreme Light Infrastructure

ELI and ELI-Beamlines



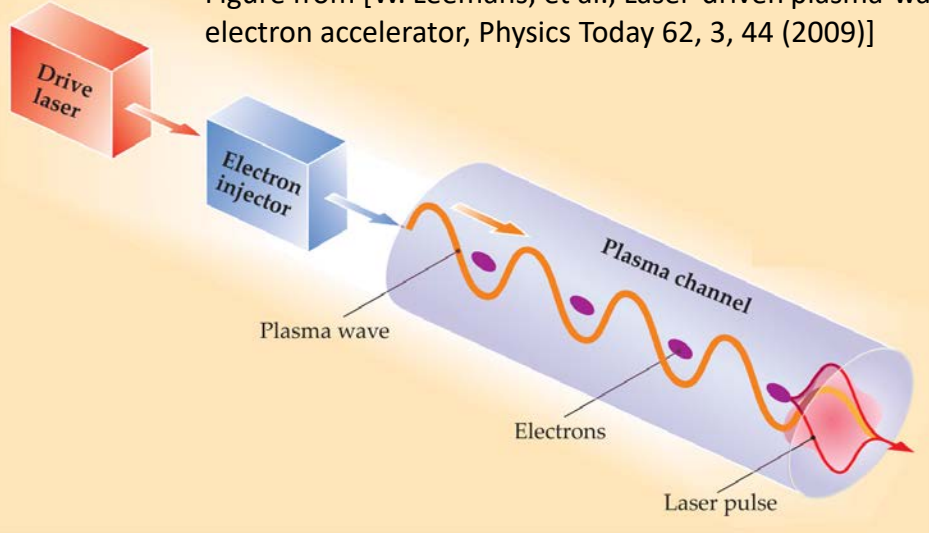
Figures from [S. Weber, et al., P3: An installation for high-energy density plasma physics and ultra-high intensity laser-matter interaction at ELI-Beamlines, matter and Radiation at Extremes, 2 (2017) 149-176]

- Extreme Light Infrastructure, ELI, is intended as an open user facility for laser-based research.
- ELI is composed of three institutes with different specializations. They are located in Czech Republic, Hungary and Romania.
- ELI-Beamlines aim to deliver unprecedented ultrashort and ultra-intense laser pulses* for various applications.

*: with ultra-high peak powers of 10 PW

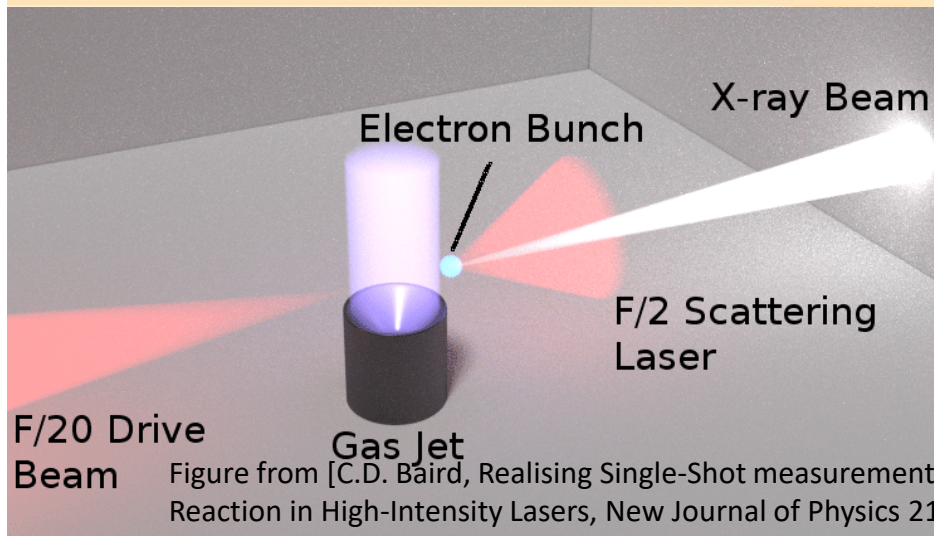
Electron acceleration and laser Compton scattering

Figure from [W. Leemans, et al., Laser-driven plasma-wave electron accelerator, Physics Today 62, 3, 44 (2009)]



An intense laser pulse traversing a plasma exciting a plasma wave in its wake.

The wave accelerates electrons injected from an external source or trapped from the plasma.



A schematic of an inverse Compton scattering setup. The scattered electrons produce a X-ray beam.

X-ray can be transferred into visible light by filters. Use detectors (industry cameras) to collect the data.

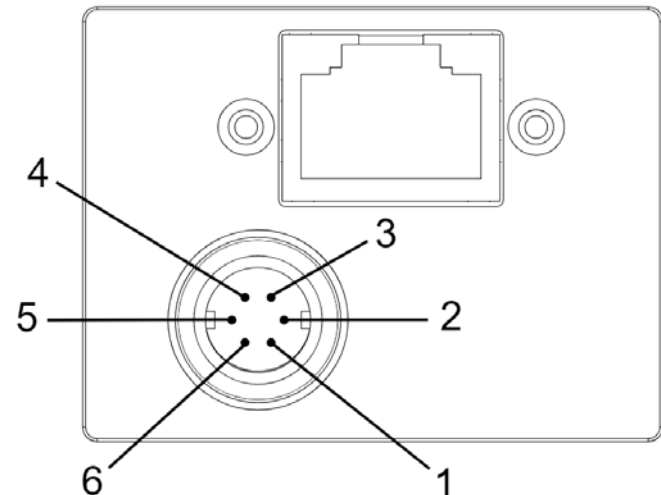
Figure from [C.D. Baird, Realising Single-Shot measurements of Quantum Radiation Reaction in High-Intensity Lasers, New Journal of Physics 21 (5) 2018]

Detectors used

Figures from [Basler](#)



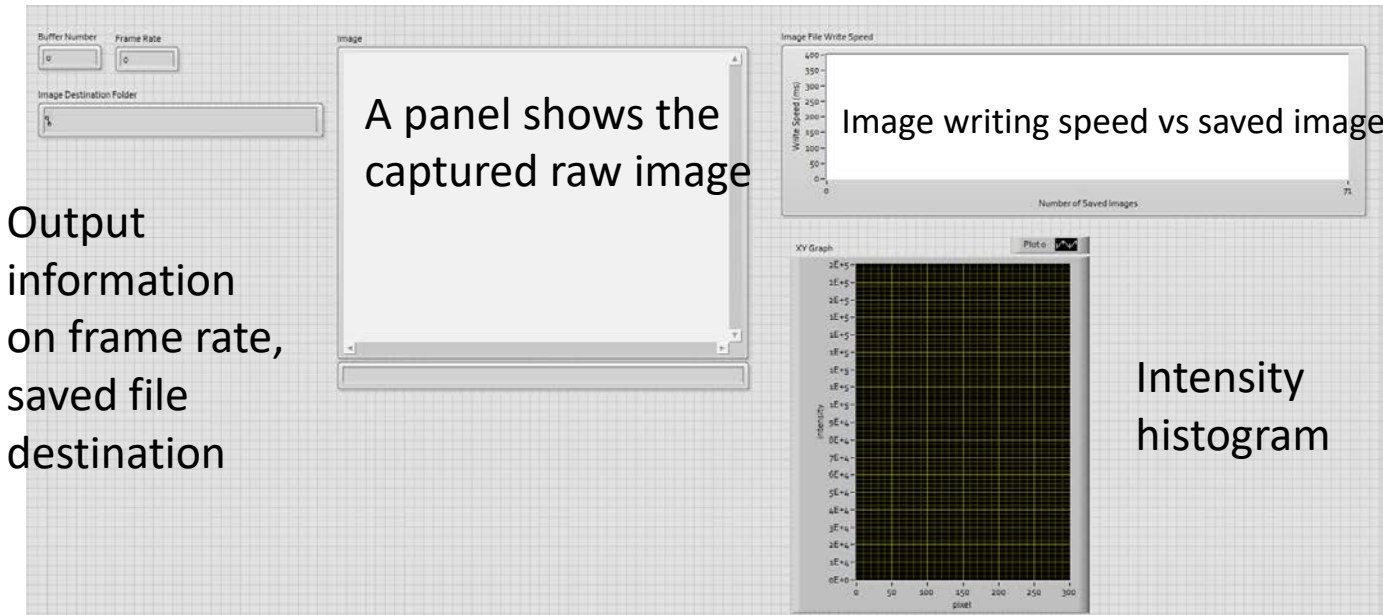
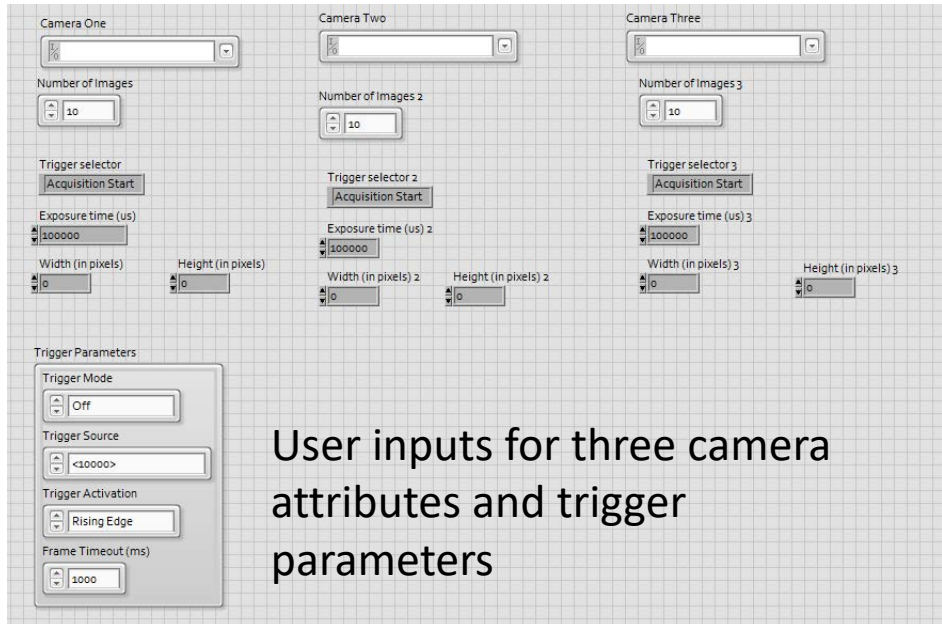
- One of Basler detectors is a camera, acA4096-11gm, whose spec:
 - resolution (pixel x pixel): 4096 x 2168
 - sensor type: CMOS
 - frame: 13.1 fps
 - Mono
 - Image Data interface: Gigabit Ethernet (1000 Mbit/s)



Camera acquisition with LabVIEW

The DAQ system with LabVIEW controls three industry cameras* to observe the experiments.

*: Basler GigE camera with CMOS sensor.



A Python interface is open in this LabVIEW program, which is for developing machine learning solution:

- For coherent control of plasma dynamics
- For pre-selection of captured image

Thanks for your attention

Backup

Elementary particles and fundamental forces

Standard Model of Elementary Particles

three generations of matter (fermions)			interactions / force carriers (bosons)	
I	II	III		
mass charge spin	$\approx 2.2 \text{ MeV}/c^2$ $\frac{2}{3}$ $\frac{1}{2}$ u up	$\approx 1.28 \text{ GeV}/c^2$ $\frac{2}{3}$ $\frac{1}{2}$ c charm	$\approx 173.1 \text{ GeV}/c^2$ $\frac{2}{3}$ $\frac{1}{2}$ t top	g gluon
mass charge spin	$\approx 4.7 \text{ MeV}/c^2$ $-\frac{1}{3}$ $\frac{1}{2}$ d down	$\approx 96 \text{ MeV}/c^2$ $-\frac{1}{3}$ $\frac{1}{2}$ s strange	$\approx 4.18 \text{ GeV}/c^2$ $-\frac{1}{3}$ $\frac{1}{2}$ b bottom	γ photon
mass charge spin	$\approx 0.511 \text{ MeV}/c^2$ -1 $\frac{1}{2}$ e electron	$\approx 105.66 \text{ MeV}/c^2$ -1 $\frac{1}{2}$ μ muon	$\approx 1.7768 \text{ GeV}/c^2$ -1 $\frac{1}{2}$ τ tau	Z Z boson
mass charge spin	$<1.0 \text{ eV}/c^2$ 0 $\frac{1}{2}$ ν_e electron neutrino	$<0.17 \text{ MeV}/c^2$ 0 $\frac{1}{2}$ ν_μ muon neutrino	$<18.2 \text{ MeV}/c^2$ 0 $\frac{1}{2}$ ν_τ tau neutrino	W W boson

Figure from [wiki](#)

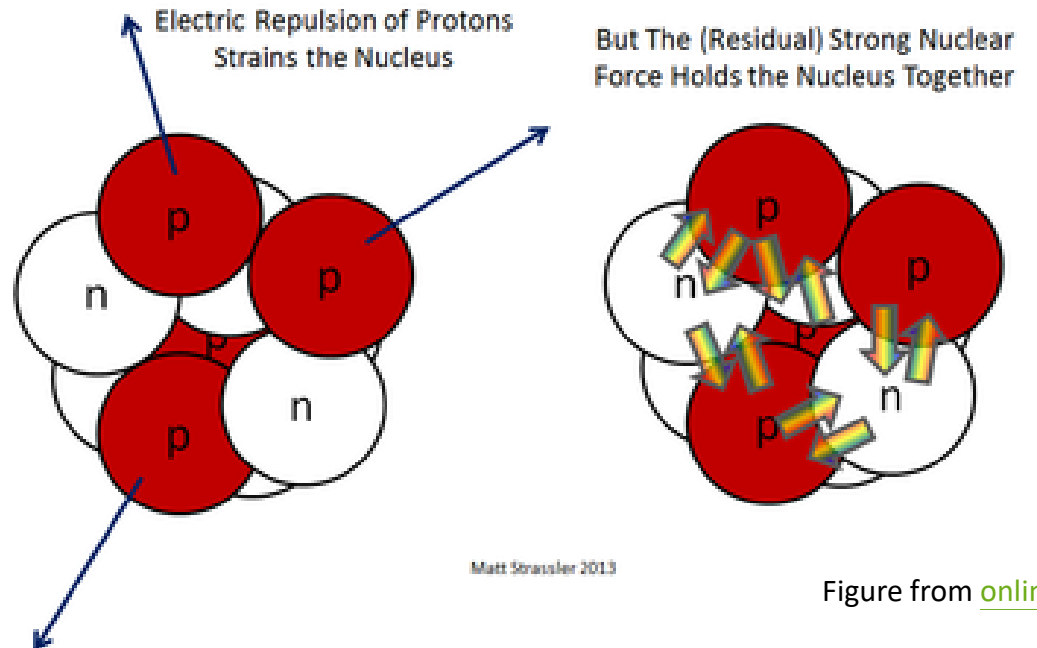


Figure from [online](#)

QCD phase diagram and quark-gluon plasma (QGP)

Because of the asymptotic freedom property of QCD, one can expect a phase of matter where quarks and gluons move freely → quark-gluon plasma (QGP)

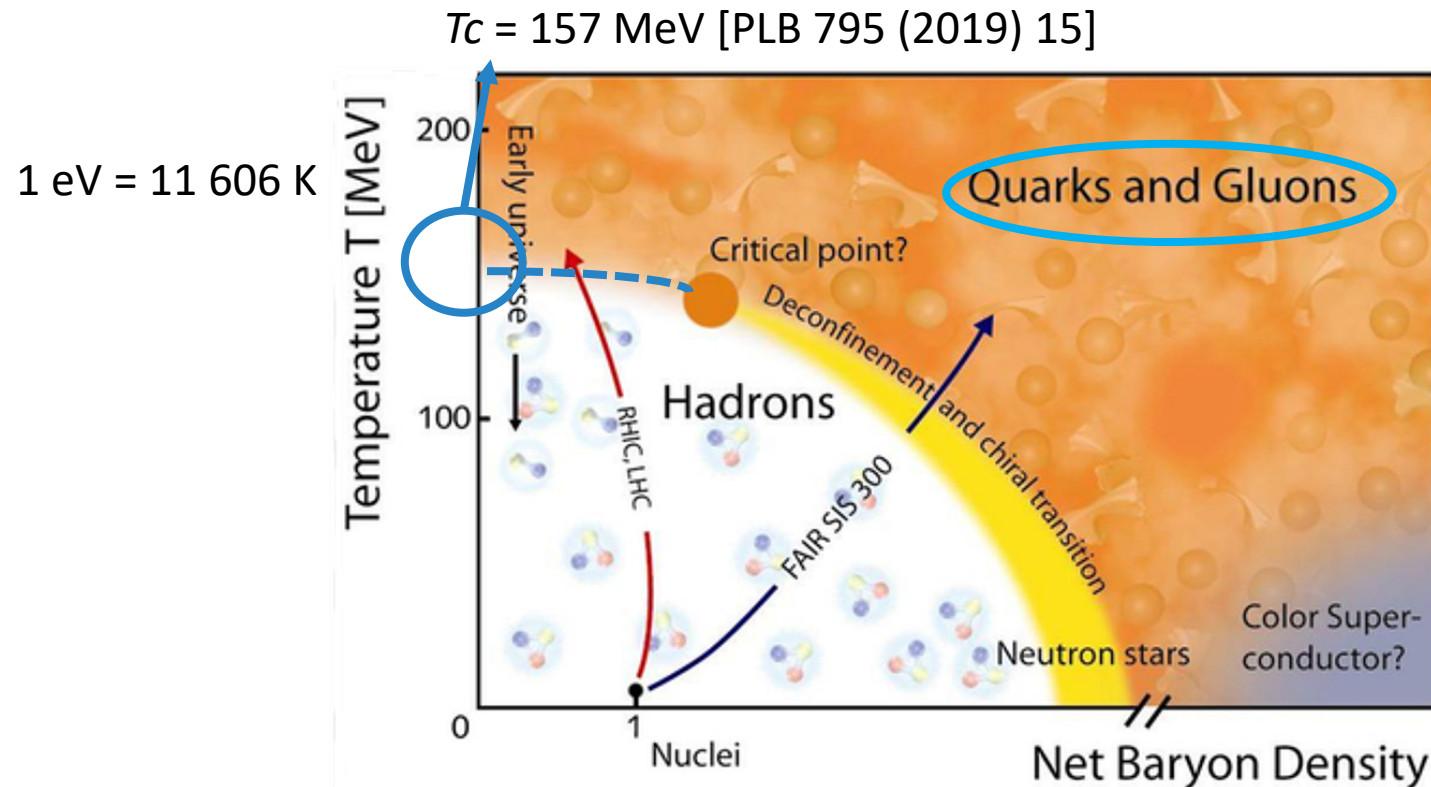


Figure from [Larry McLerran,
Braz.J.Phys. 37:861-866, 2007]

QCD matter phase diagram:

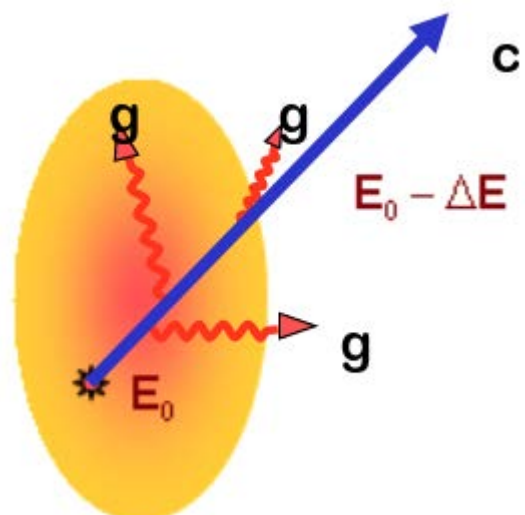
- A QGP is created at high T and/or high net baryon density.
- QGP can be achieved by using heavy-ion collisions.

Probes of the QGP (2)

- **Open heavy-flavor production**

- Charm and beauty quarks are produced in initial hard scattering prior to the formation of the QGP → heavy quarks experience the full system evolution.
- Heavy quarks interact with the QGP → heavy quarks are sensitive to **parton energy loss mechanisms**.

Visualization by M. Djordjevic and M. Gyulassy at Columbia University.



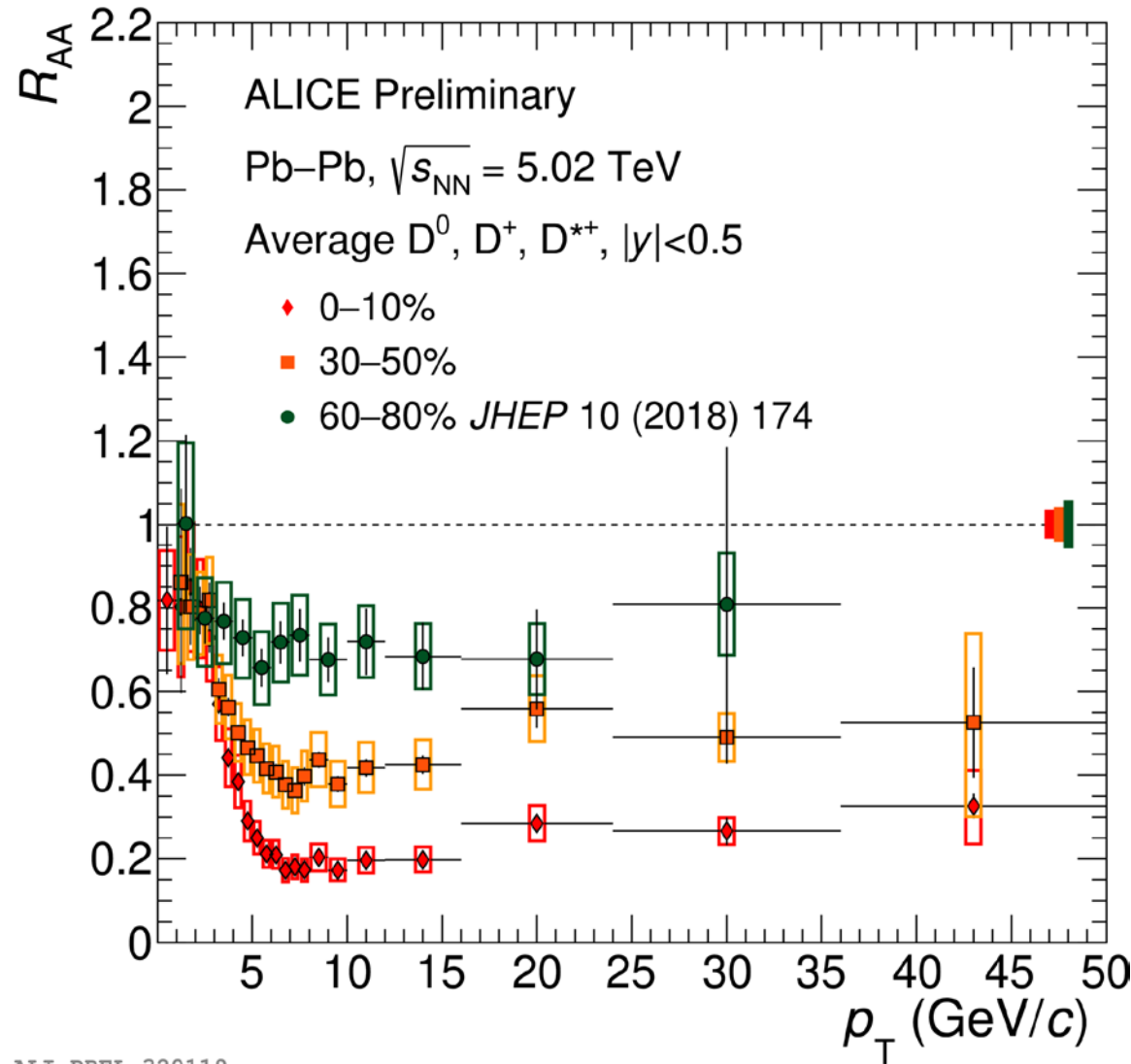
Energy loss due to the interaction of the heavy quark with the medium

Probes of the QGP (3)

- Nuclear modification factor R_{AA} is usually used for observing the hard probe yield modification in heavy-ion collisions w.r.t hadron-hadron collisions.

$$R_{AA} = \frac{Y_{AA}}{\langle T_{AA} \rangle \cdot \sigma_{pp}}$$

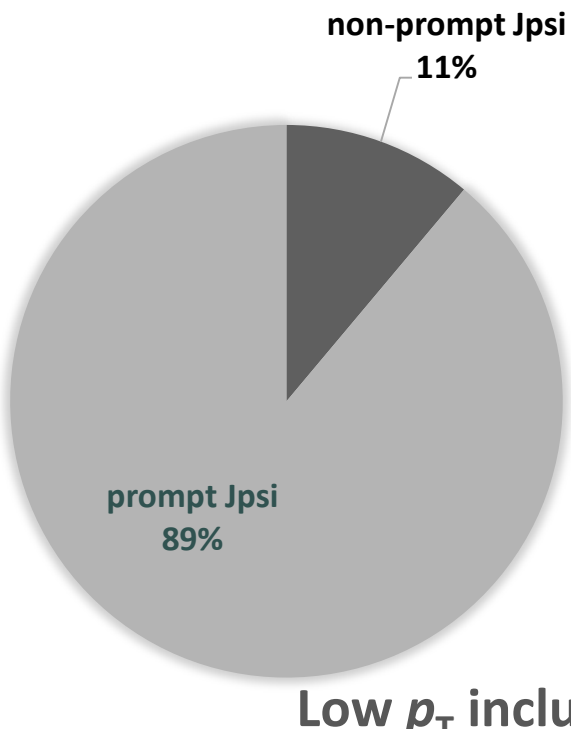
- Y_{AA} is the invariant yield in nucleus-nucleus (AA) collisions.
- σ_{pp} is the cross section in hadron-hadron (pp) collisions at the same energy.



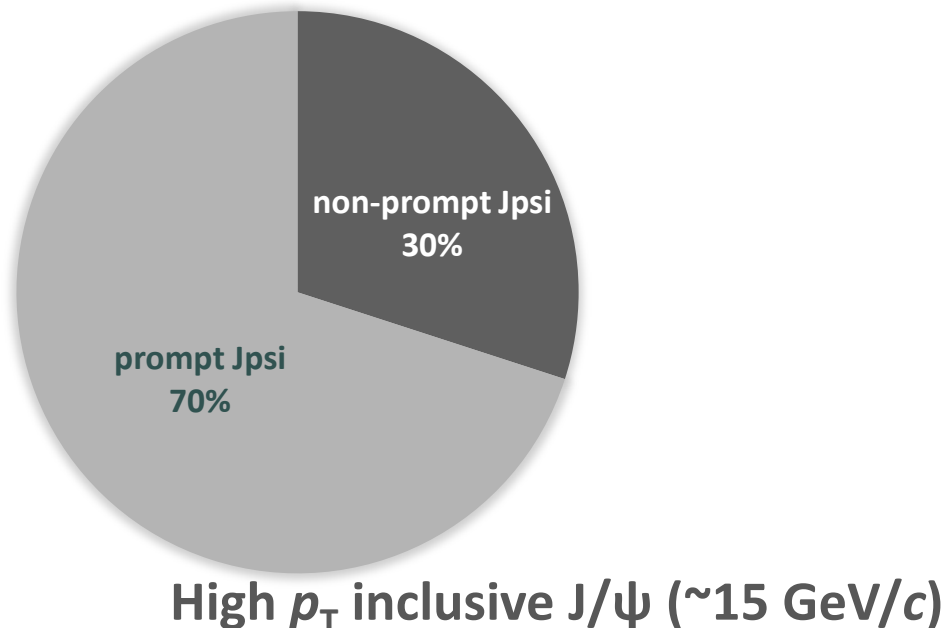
Charmonium (1)

- Charmonium production

- A charmonium consists of a c and anti- c quarks.
- A $c\bar{c}$ pair is produced in initial hard scattering (~ 0.07 fm) prior to the formation of the QGP (~ 0.1 - 1 fm/ c) [Eur. Phys. J. C 76 (2016) 3, 107] → it experiences the full system evolution.



Low and high p_T values
from [arXiv: 1903.09185]



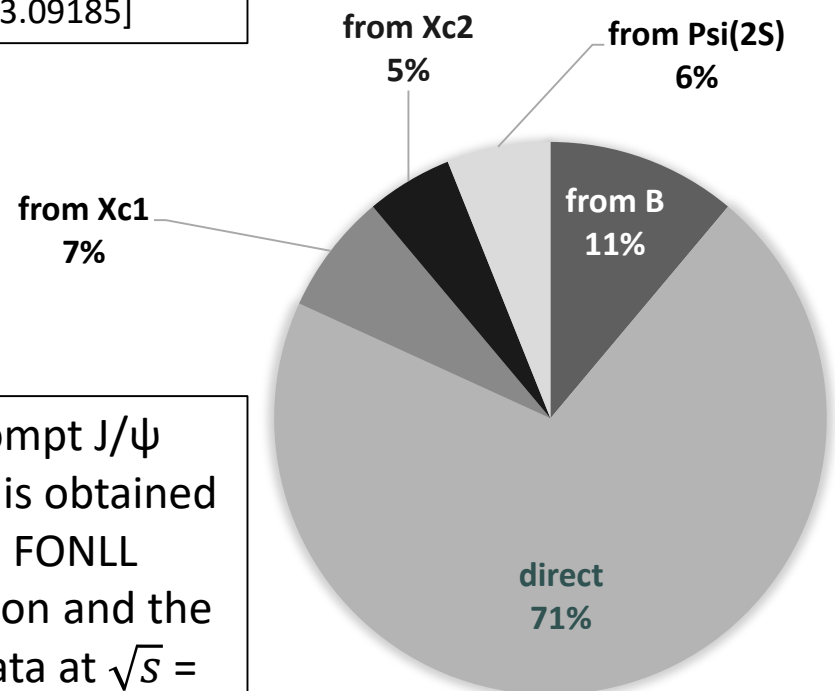
Non-prompt J/ψ
fraction is obtained
by using FONLL
calculation and the
ALICE data at $\sqrt{s} =$
 5.02 TeV.

Charmonium (2)

- Charmonium production

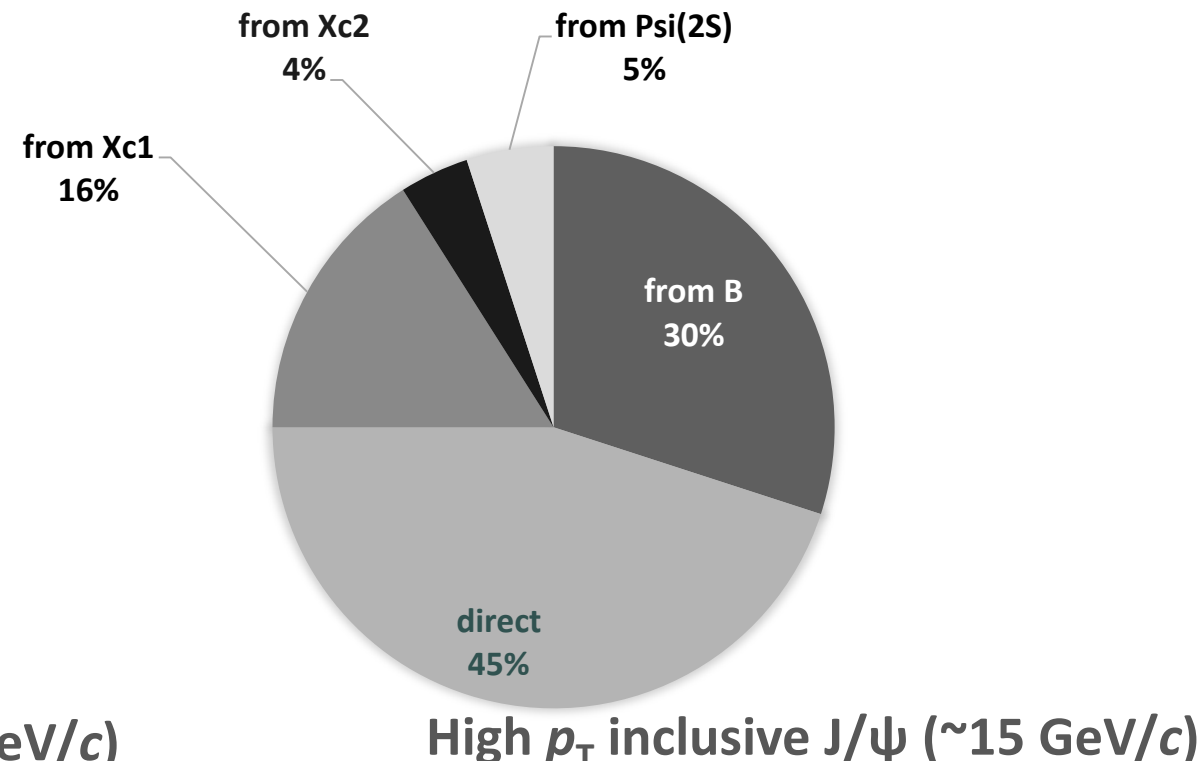
- A charmonium consists of a c and anti- c quarks.
- A $c\bar{c}$ pair is produced in initial hard scattering (~ 0.07 fm) prior to the formation of the QGP (~ 0.1 - 1 fm/ c) [Eur. Phys. J. C 76 (2016) 3, 107] → it experiences the full system evolution.

Prompt J/ψ fraction from
[arXiv: 1903.09185]



Non-prompt J/ψ fraction is obtained by using FONLL calculation and the ALICE data at $\sqrt{s} = 5.02$ TeV.

Low p_T inclusive J/ψ (~ 2 GeV/ c)



High p_T inclusive J/ψ (~ 15 GeV/ c)

Charmonium in large system

- Large system refers to Pb-Pb collisions.
- Charmonium production in Pb-Pb collisions is one of the probes of the QGP.

Charmonium suppression:

- Prompt charmonium production suppressed by **color screening** in QGP.
- Different charmonium binding energy → **sequential suppression** with increasing medium temperature.

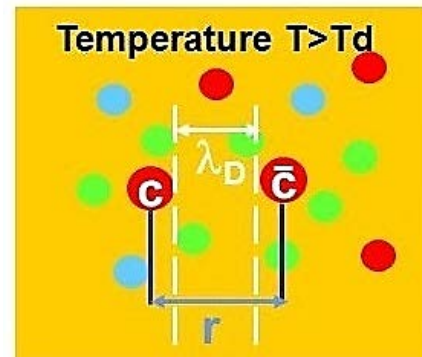
T : medium temperature

T_d : dissociation temperature

r : binding radius

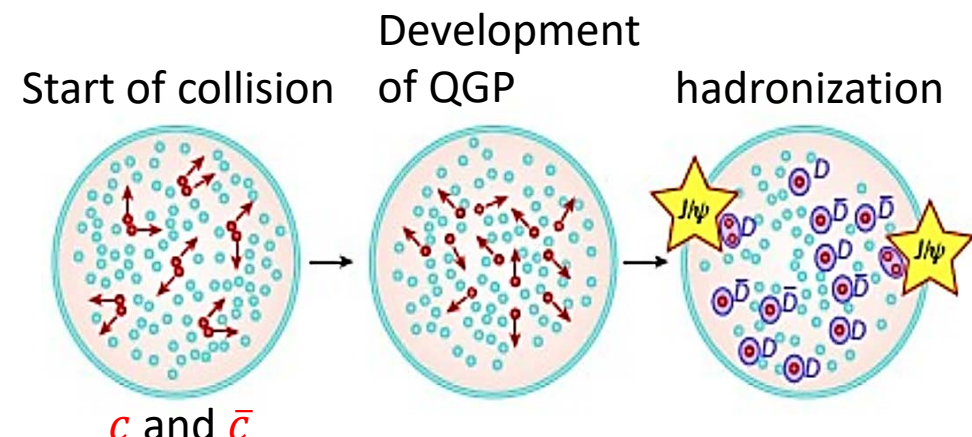
λ_D : screening radius

T_c : critical temperature



(Re)generation:

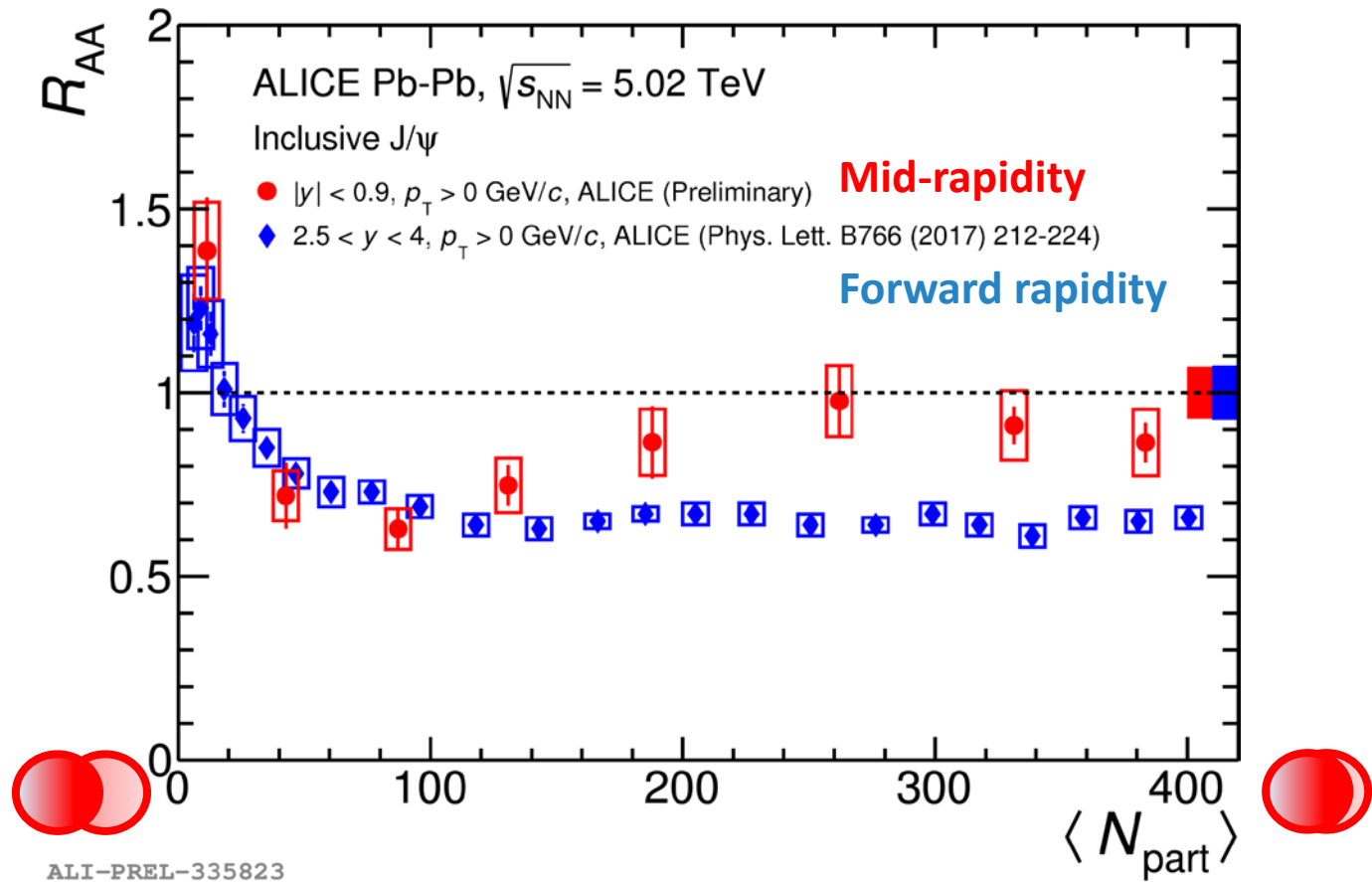
- At the LHC, the charm quark density is large (number of $c\bar{c}$ pairs ≈ 100 [J. Phys. G 41 (2014) 124006]).
- In the medium, deconfined charm quarks can form a charmonium.



state	J/ ψ	$\psi(2S)$
T_d	$1.2 T_c$	$\leq T_c$

[Eur.Phys.J.C 71 (2011) 1534]

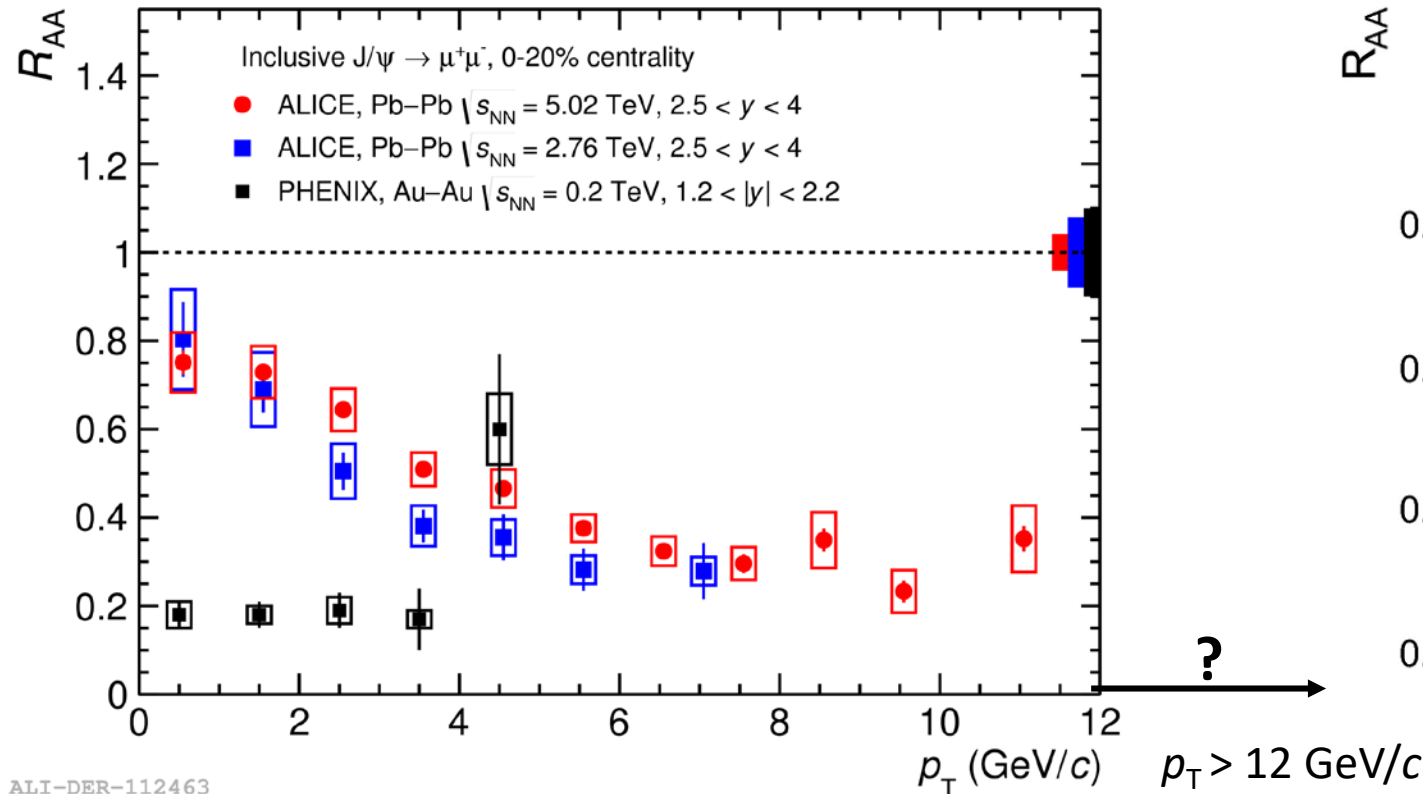
$\text{J}/\psi R_{\text{AA}}$ at the LHC (ALICE)



The R_{AA} at mid-rapidity is higher than the R_{AA} at forward rapidity for $\langle N_{\text{part}} \rangle > 200$:

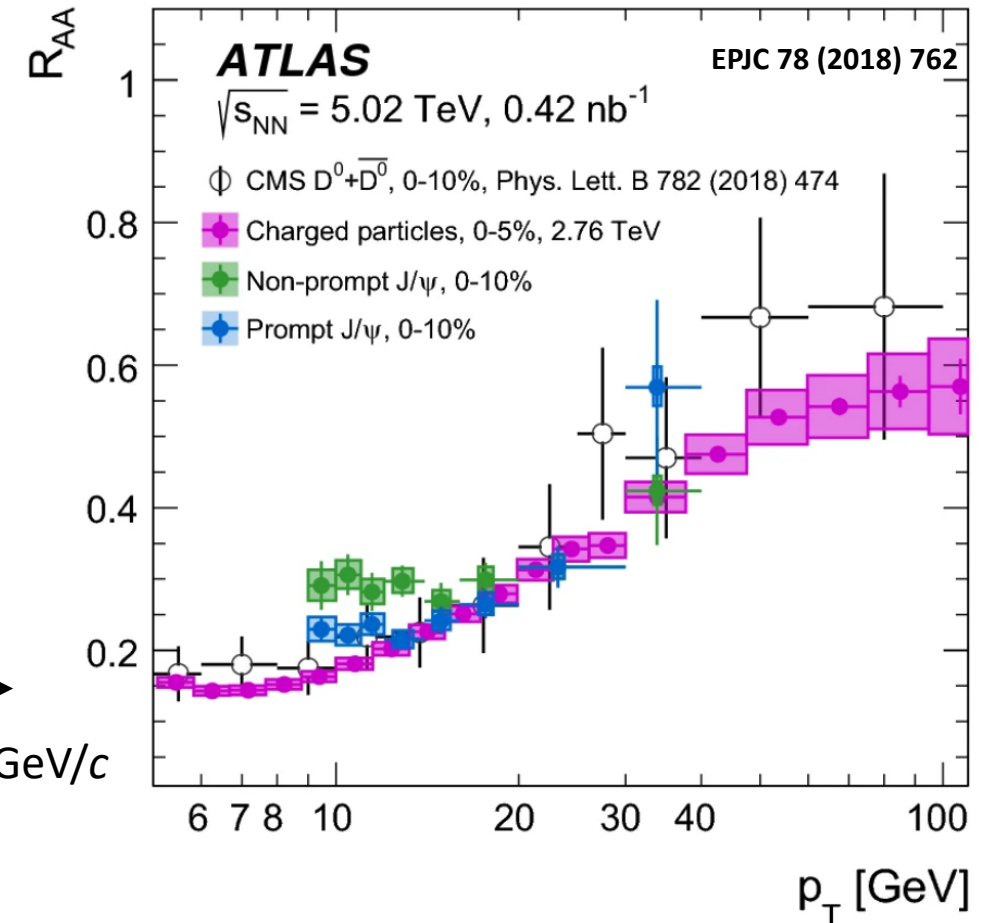
- $c\bar{c}$ density is larger at mid-rapidity
- Hint of (re)generation

R_{AA} at RHIC (PHENIX) and LHC (ALICE, ATLAS and CMS)



ALI-DER-112463

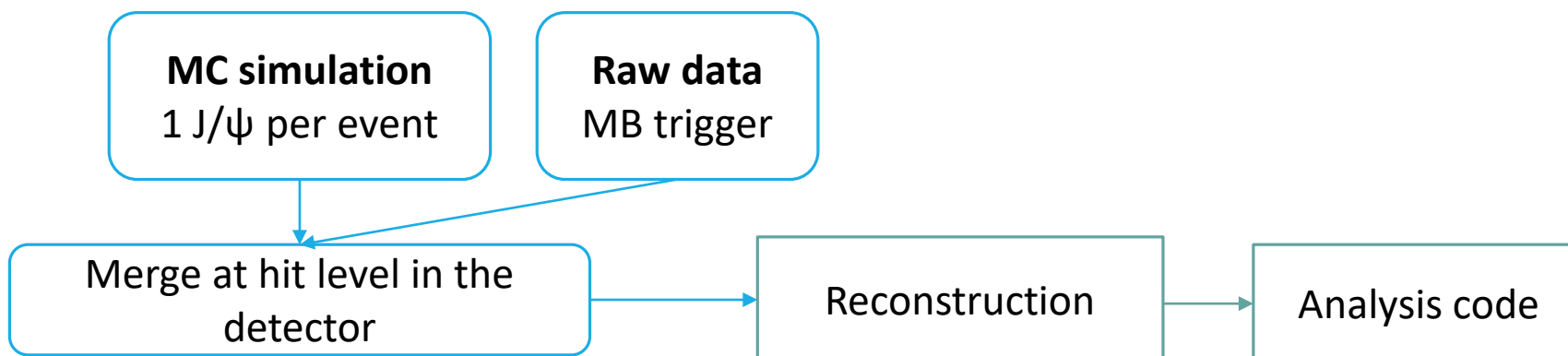
$p_T < 6 \text{ GeV}/c$: $R_{AA}^{J/\psi}$ increases towards low p_T and $R_{AA}^{J/\psi}$ larger at LHC than at RHIC → hint of regeneration.



$p_T \geq 15 \text{ GeV}/c$: $R_{AA}^{J/\psi} \sim R_{AA}^{\text{charged}}$ → a sign of energy loss → interplay between color screening and energy loss at high p_T .

Embedded MC simulation of Pb-Pb collisions

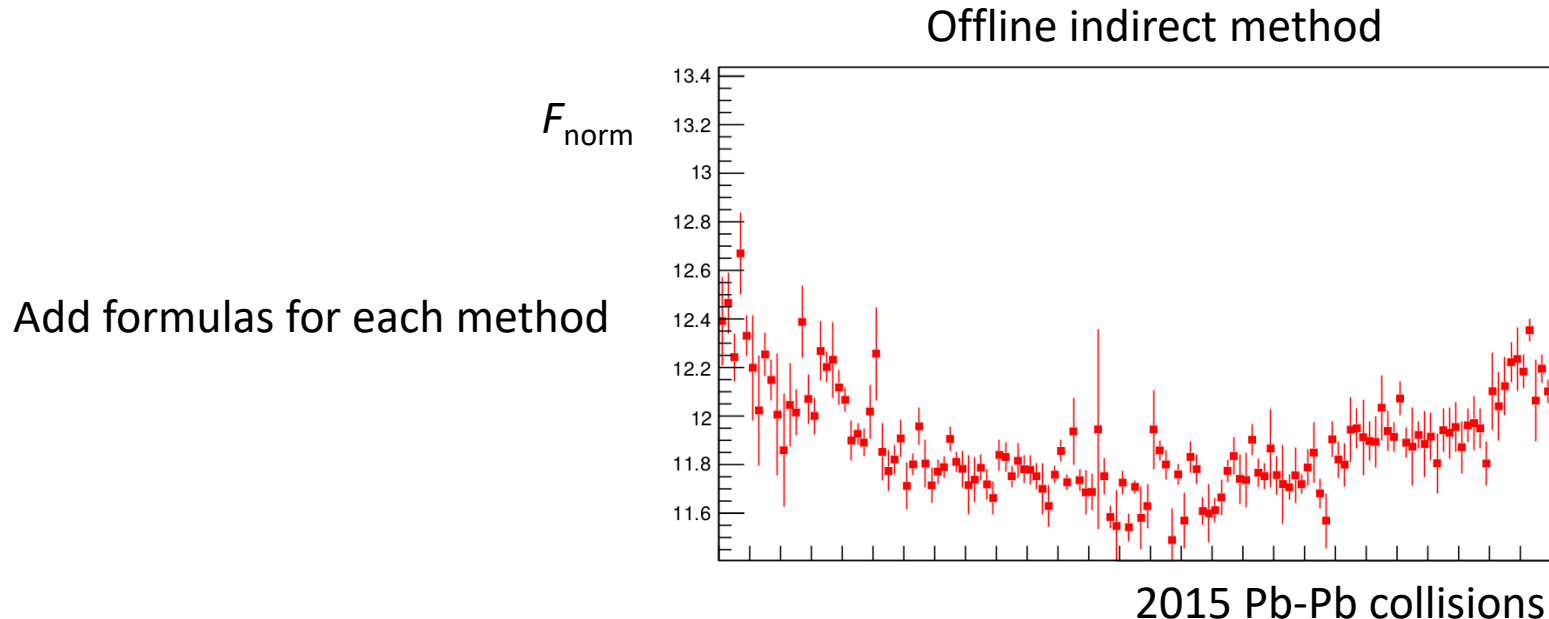
Principle of an embedded MC simulation



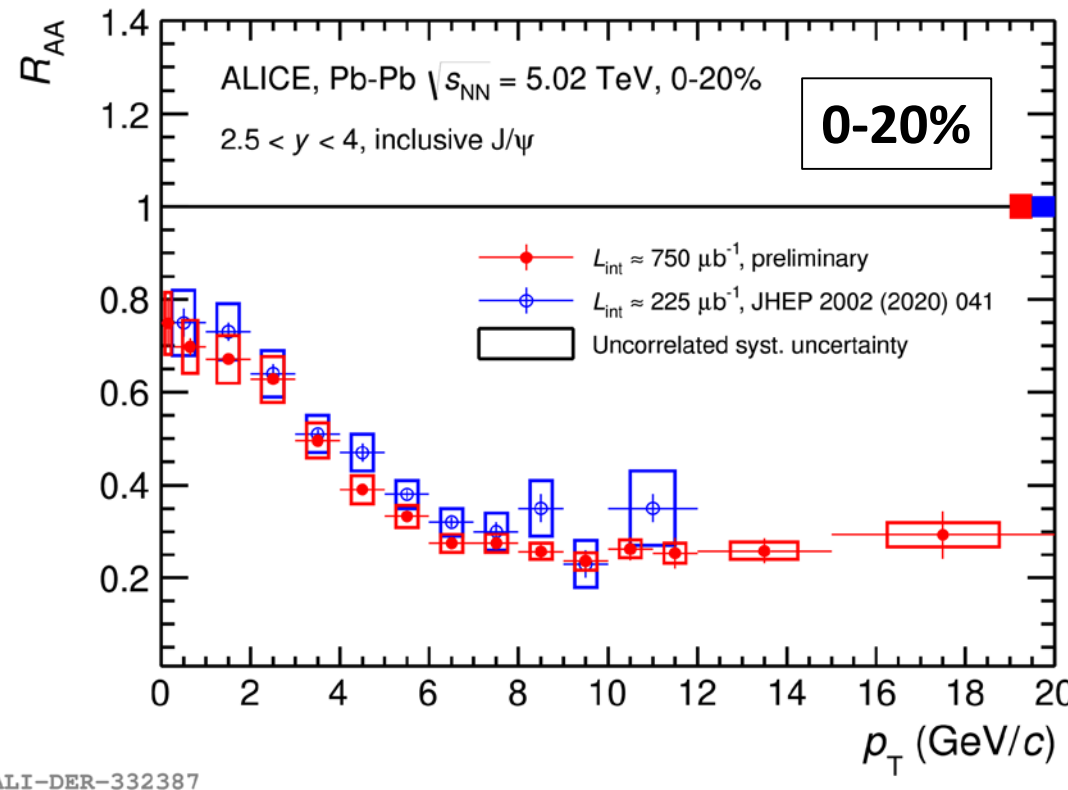
Embedding simulation: merge at hit level raw data and pure signal-> allow to simulate the high occupancy of the detectors

Normalization factor and MB events

- In the **Pb-Pb data analysis**, three methods, offline (in)direct and online methods, are used. The final F_{norm} is the average of the values obtained from different methods.
- The systematic uncertainty on F_{norm} is estimated from relative difference between different methods.
- Number of minimum bias events are calculated with: $N_{\text{MB}} = F_{\text{norm}} \times N_{\text{CMUL7}}$

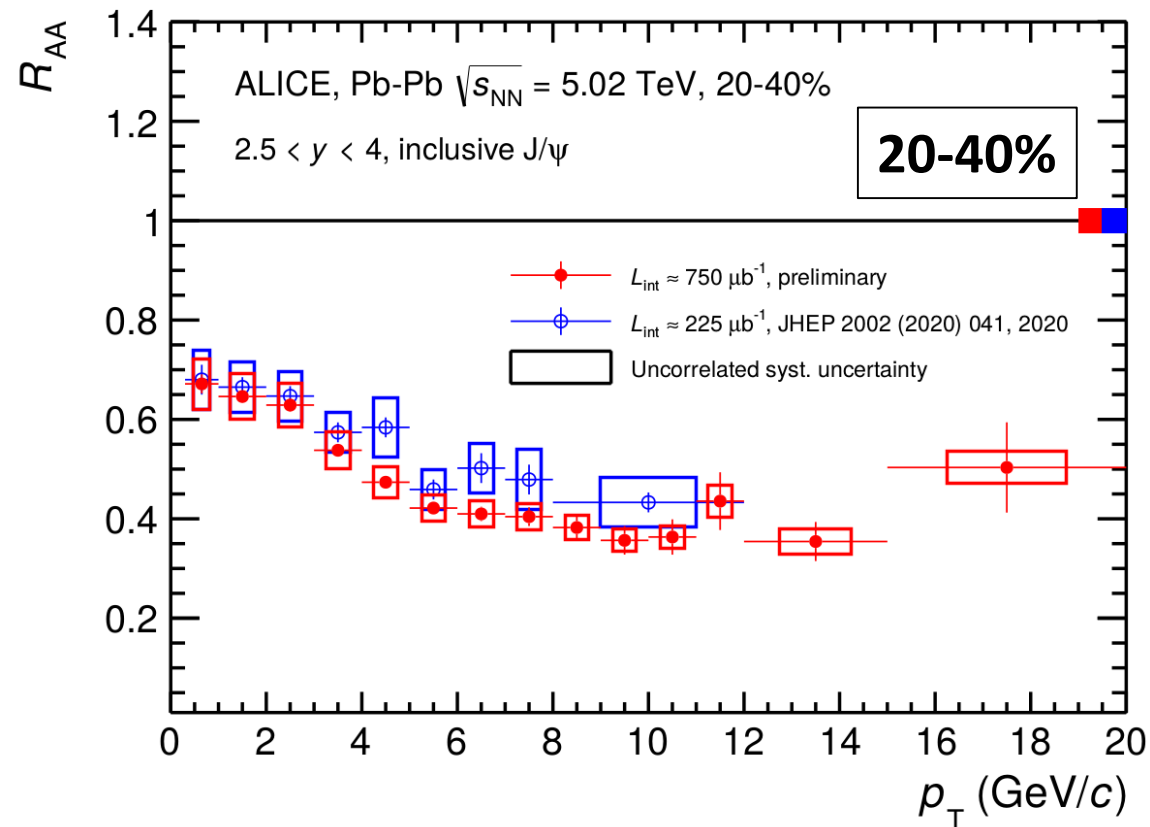


$\text{J}/\psi R_{\text{AA}}$ as a function of p_{T} in Pb-Pb (1)

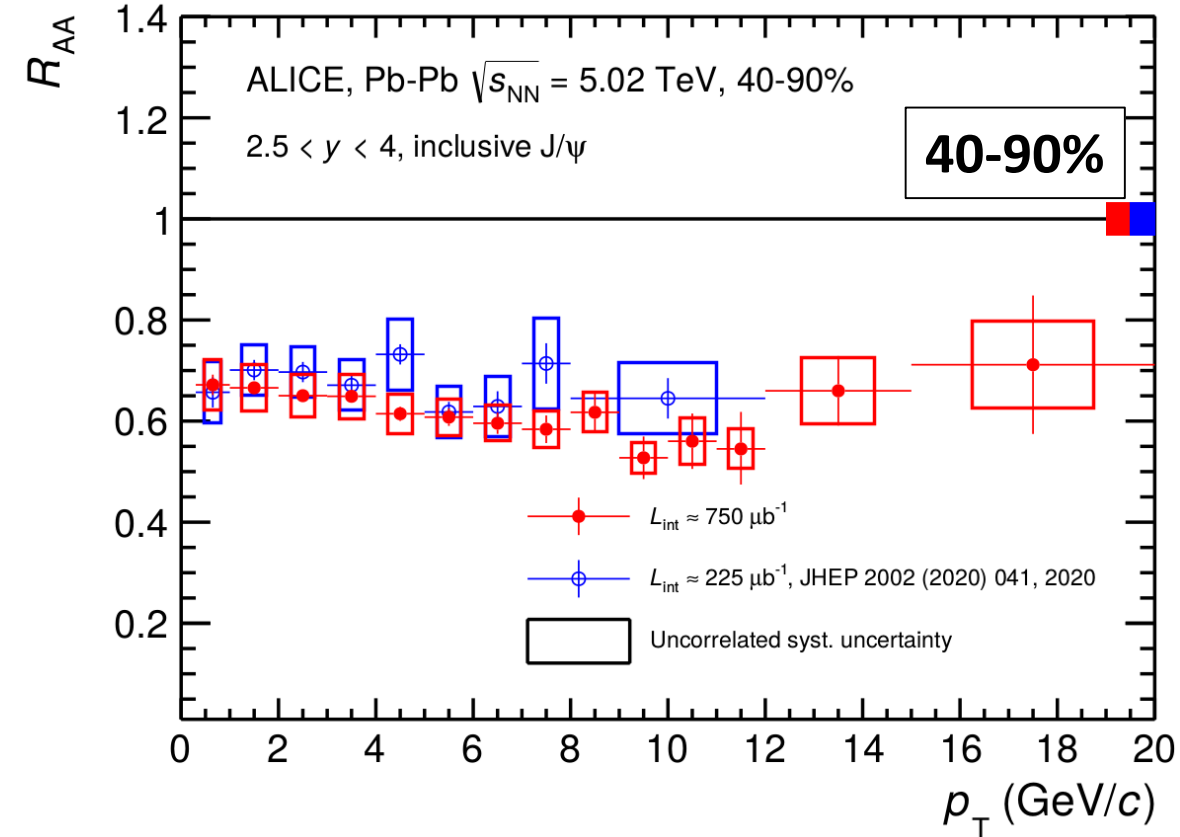


- Agreement with [previous measurement](#) from ALICE
- [New measurement](#) extends to higher p_{T}

$\text{J}/\psi R_{\text{AA}}$ as a function of p_{T} in Pb-Pb (2)

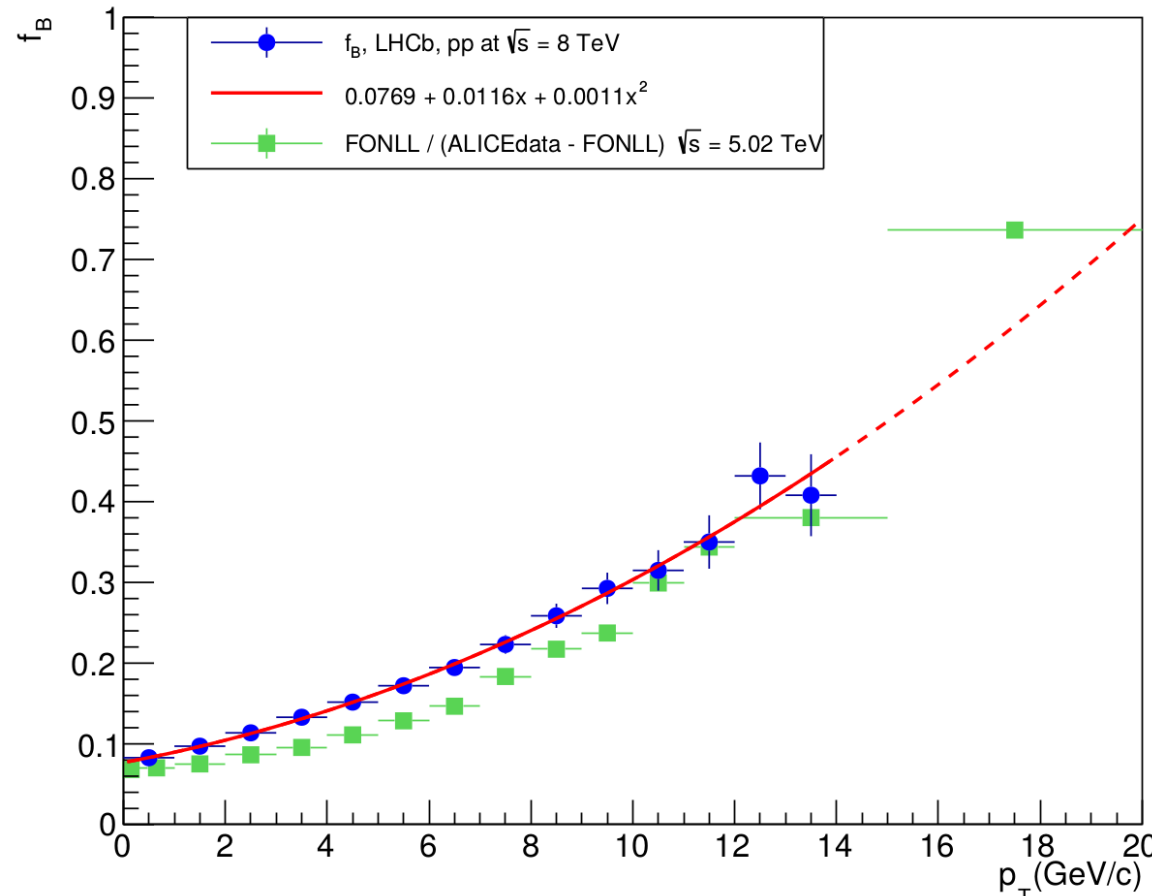


- Agreement with the previous measurement from ALICE
- R_{AA} increases towards low p_{T}
- R_{AA} stays about 0.4 for $6 < p_{\text{T}} < 20 \text{ GeV}/c$

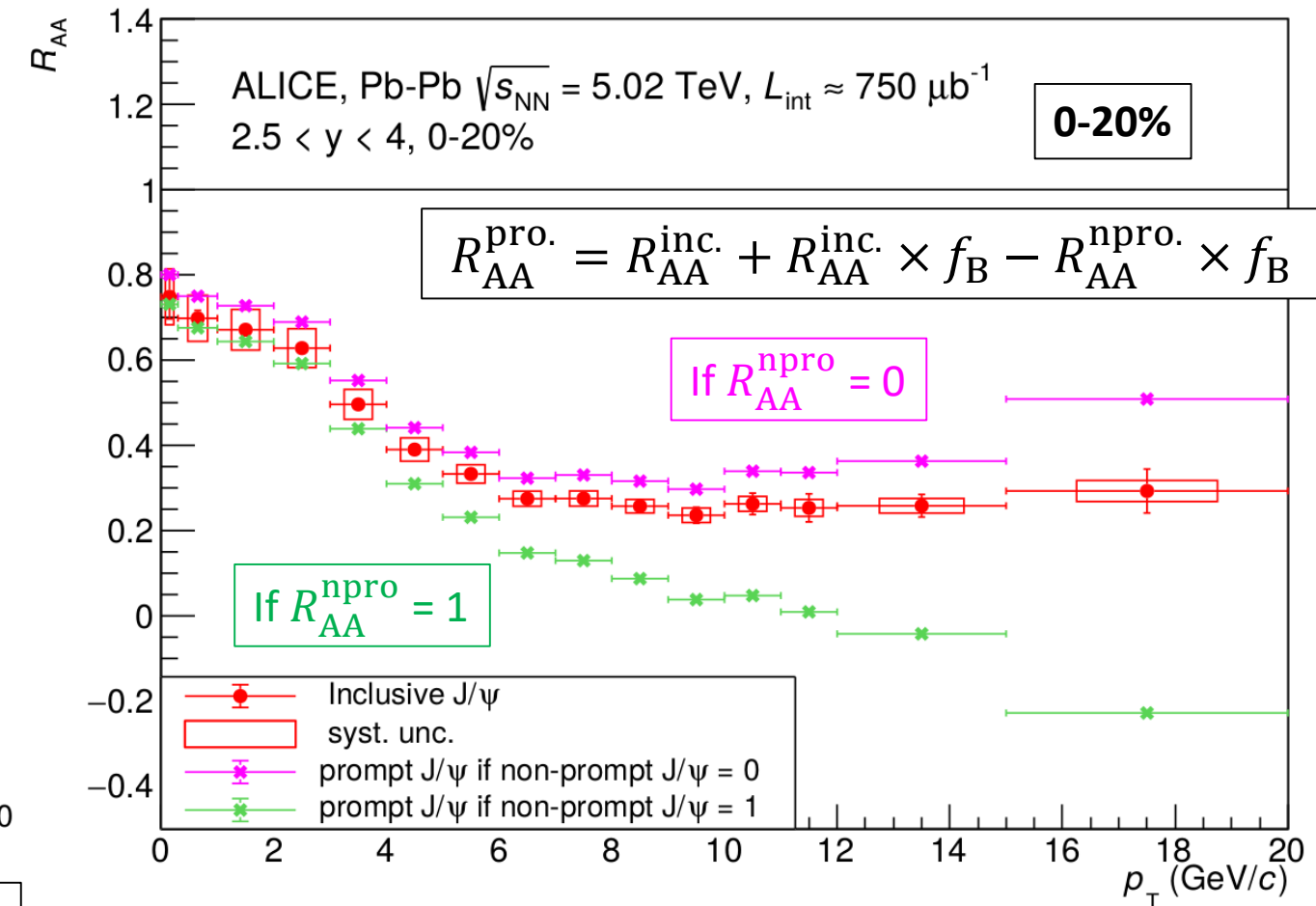


- Agreement with the previous measurement from ALICE
- R_{AA} remains constant between 0.6 and 0.7 over p_{T}

Effect of non-prompt J/ ψ on R_{AA} (1)

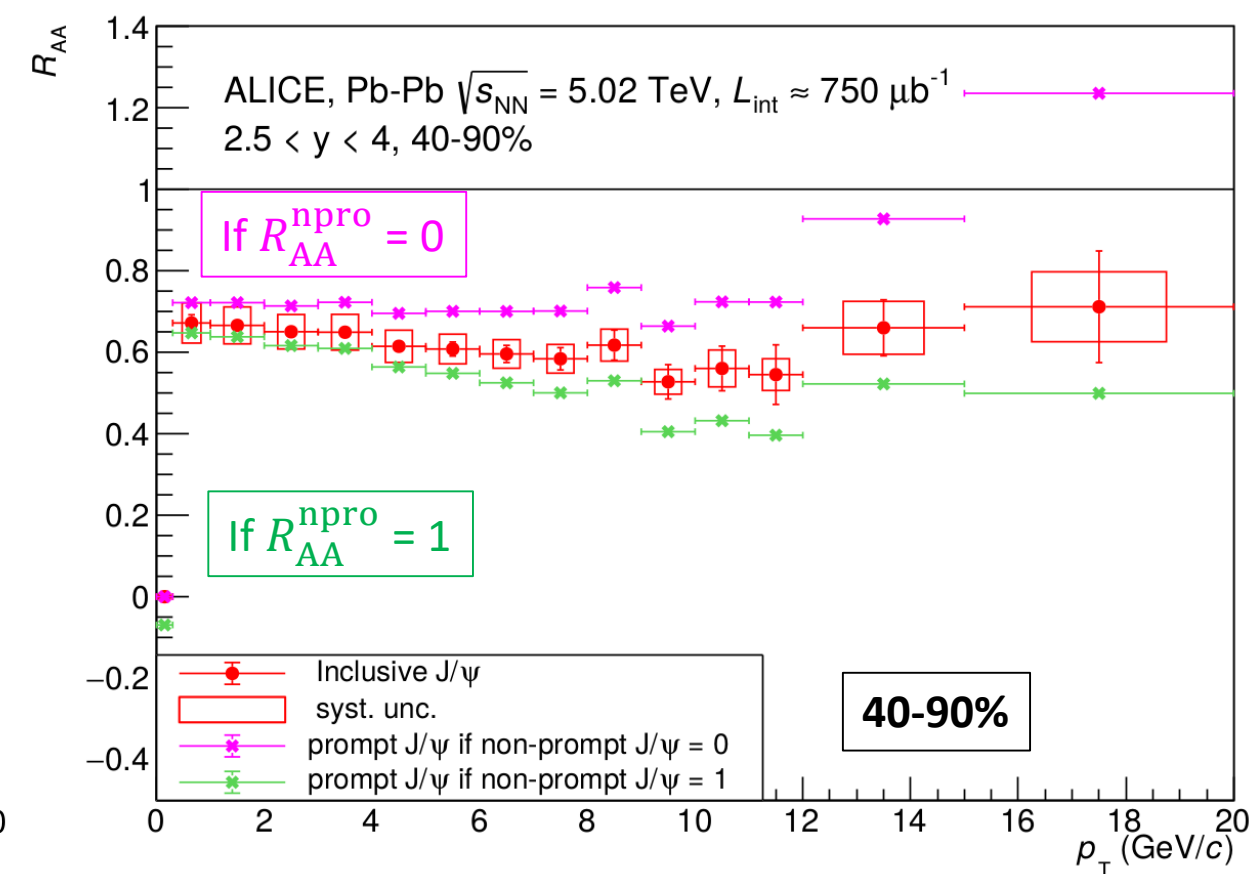
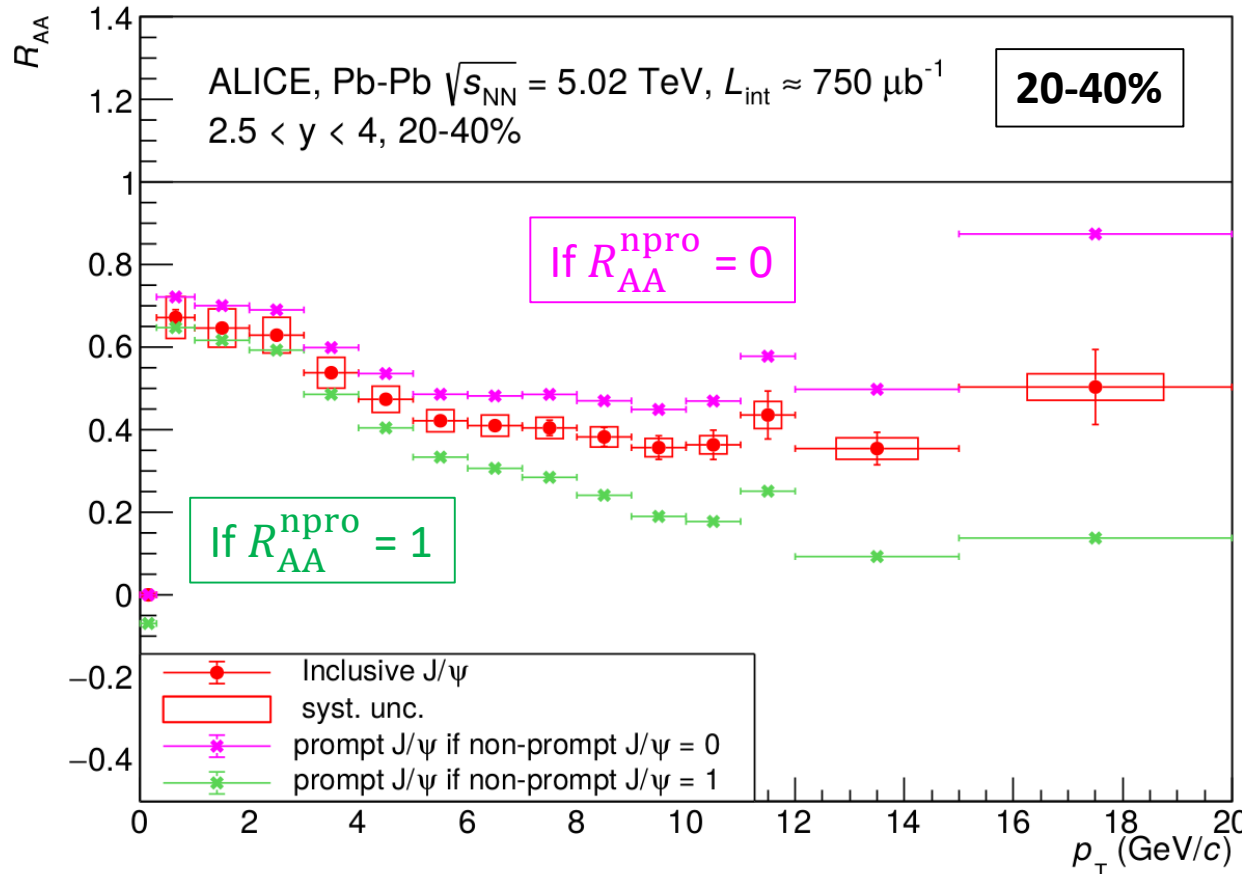


The two f_B are similar for $p_T > 10$ GeV/c while the f_B at $\sqrt{s} = 5.02$ TeV is lower for $p_T \leq 10$ GeV/c $\rightarrow b$ -hadron contribution is large at high p_T .



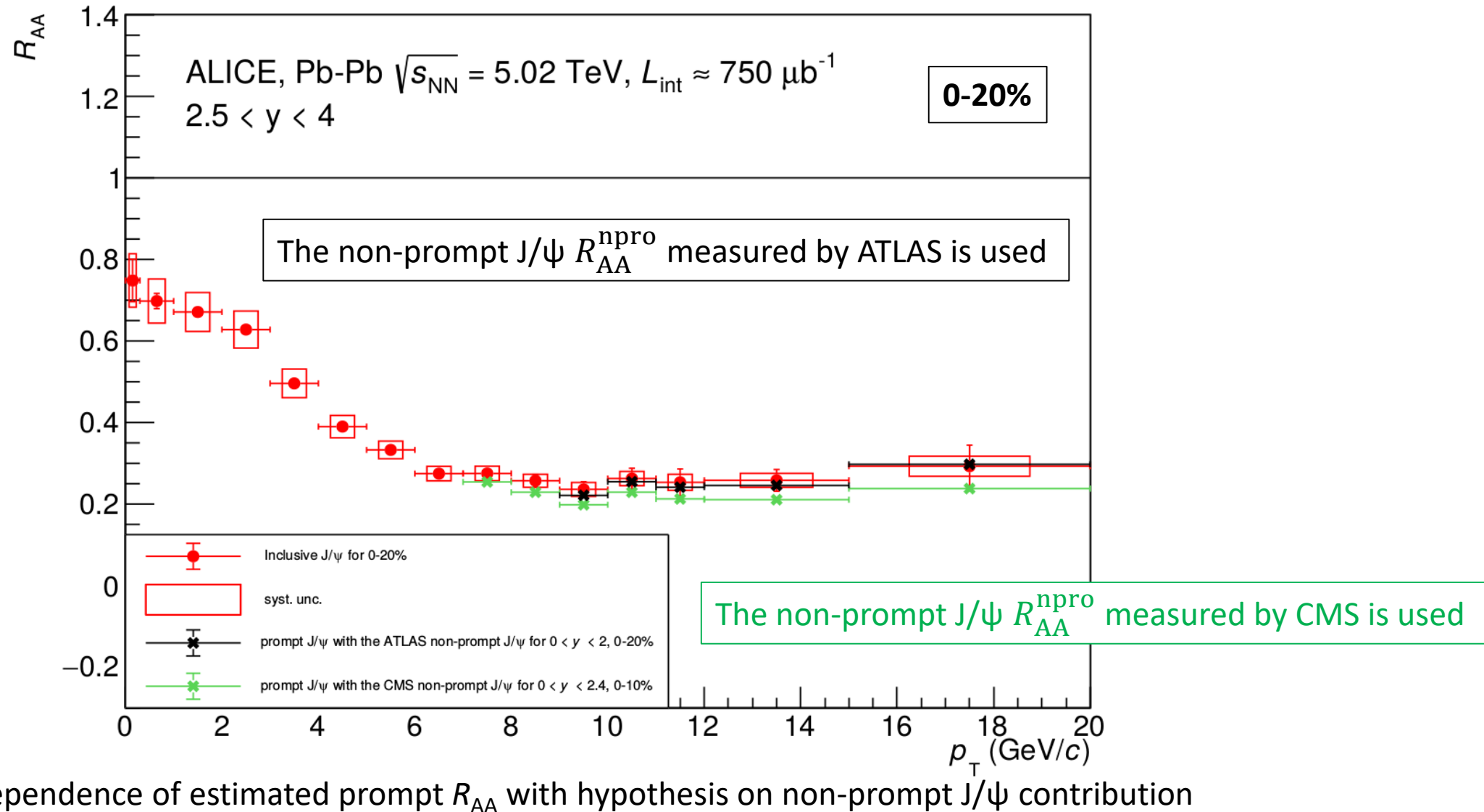
p_T dependence of estimated prompt R_{AA} with hypothesis on non-prompt J/ψ contribution

Effect of non-prompt J/ ψ on R_{AA} (2)

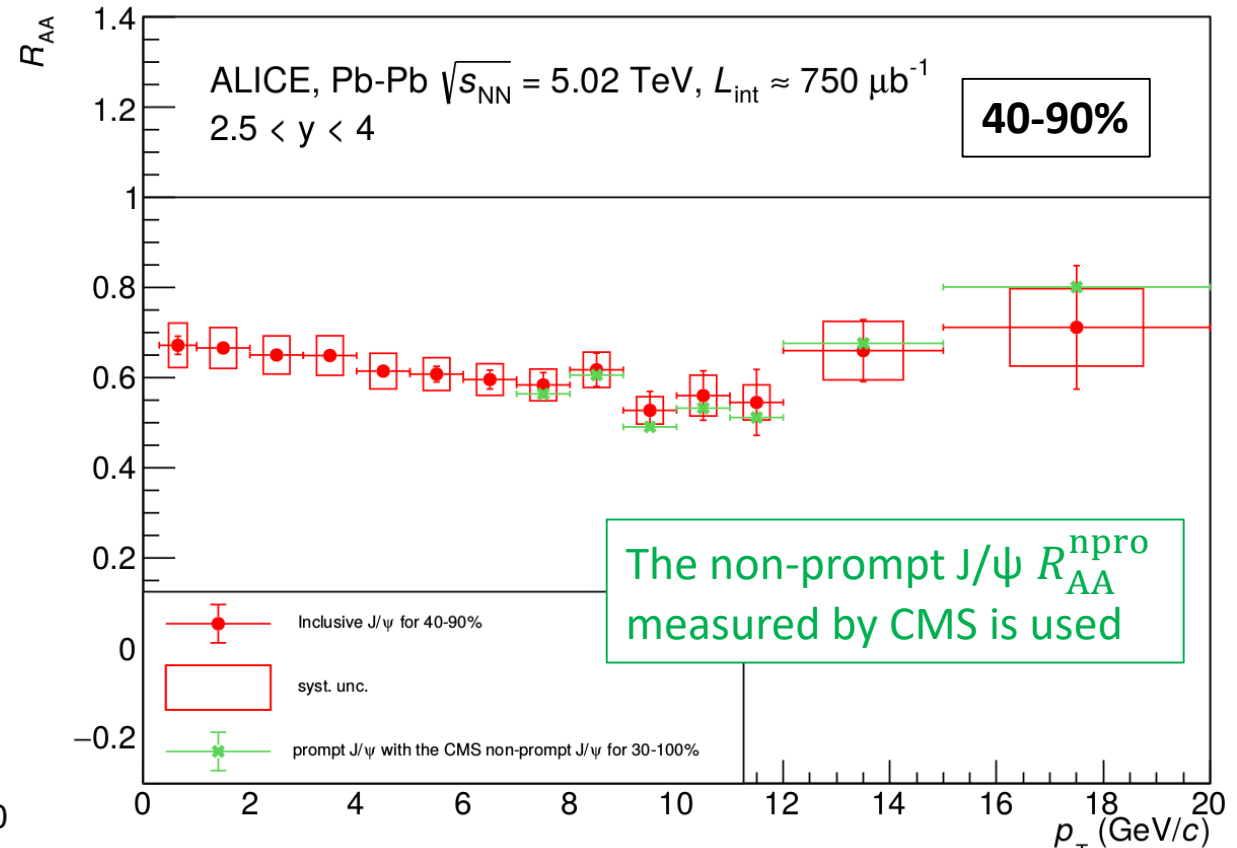
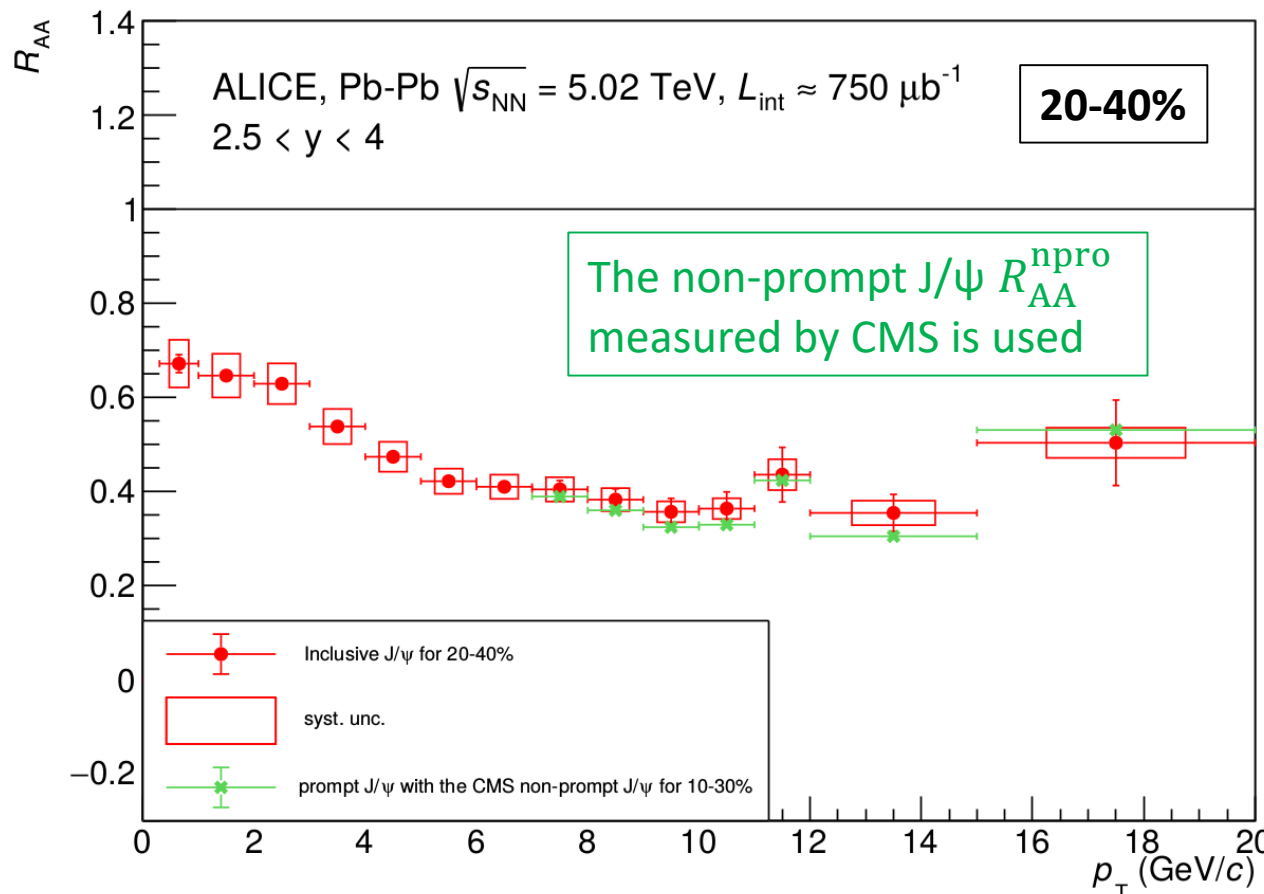


p_T dependence of estimated prompt R_{AA} with hypothesis on non-prompt J/ ψ contribution

Effect of non-prompt J/ ψ on R_{AA} (3)



Effect of non-prompt J/ ψ on R_{AA} (4)



p_T dependence of estimated prompt R_{AA} with hypothesis on non-prompt J/ ψ contribution